ON THE FAR-ZONE ELECTROMAGNETIC FIELD OF A VERTICAL AND HORIZONTAL ELECTRICAL DIPOLE OVER AN IMPERFECTLY CONDUCTING HALF-SPACE WITH EXTENSIONS TO PLASMONICS

A Thesis

by

HUNG I LIN

Submitted to the Office of Graduate and Professional Studies of
Texas A&M University
in partial fulfillment of the requirements for the degree of

MASTER OF SCIENCE

Chair of Committee,	Krzysztof A. Michalski
Committee Members,	Robert D. Nevels
	Mark Everett
	Paotai Lin
Head of Department,	Miroslav M. Begovic

August 2021

Major Subject: Electrical Engineering

ABSTRACT

The new asymptotic formulas for the radiation fields from vertical and horizontal electric dipoles over an imperfectly conducting half-space are derived using the modified saddle point method. The asymptotic formulation is assessed in comparison with the Norton-Bannister formula, King formula, and the results of rigorous numerical evaluation of the Sommerfeld integrals. From RMS errors of the numerical results of the field patterns and surface field plots, the new second-order asymptotic formulation has been found to be more accurate than the other compared formula for the problems with seawater in microwave range and gold in the visible range, especially in the plasmonic case.

ACKNOWLEDGMENTS

I would like to thank Dr. Krzysztof A. Michalski for useful advice on my research. Also, I want to thank the committee members for the valuable comments on my thesis.

TABLE OF CONTENTS

LIST OF FIGURES

LIST OF TABLES

CHAPTER I

INTRODUCTION

The electromagnetic fields from a Hertzian dipole radiating over an imperfectly conducting ground known as the Sommerfeld problem are of interest to many applications, such as near ground communication, near-field optics, wireless sensors networks, and plasmonic. Since there are no closed-form solutions for Sommerfeld integrals, many researchers derived their approximated formulas by using different integration techniques and transformations under the high conductive ground and far-field conditions [4,13,14,32,35] and some of them were reviewed by Maclean and Wu [3]. Among a variety of approximated formulas, the formulas proposed by Norton [4] are considered as the standard method that is challenged by King [32]. Nevertheless, the King formulation is equivalent to Norton's [4] and its extension by Bannister [5], which has been proved by Michalski and Jackson [33].

The leading order approximation of the Sommerfeld integrals can be obtained by using a systematic approach - saddle point (SP) method - that deforms the integration path into the steepest descent path passing through the saddle point. When the steepest descent path passes or is in the vicinity of any type of singularity, a more general method - modified saddle point (MSP) method - is applied to consider the singularity effect, which has been preferred in recent research [2]. There are two types of singularities, pole and branch point, which are in the Sommerfeld integral in the half-space problem. For the pole singularity, there are two variants of the MSP method based on the two different expansions to separate the pole from the subtractive integration kernel [7] and multiplicative integration kernel [6]. Using the multiplicative variant to remove the pole singularity is first proposed by Ott [6] and then used by Wait [8] and et al [21,37]. In the more recent studies

[2,9,10,36], the subtractive variant introduced by Van der Waerden [7,34] has been preferred. To obtain the contribution from the branch point singularity numerically, the integration around the branch-cut (BCI) technique is used [38,39]. A more efficient approach proposed by Michalski [40] is to deform the branch cut into the steepest descent path (BCP) emanating from the branch point. Then, the contribution of the branch cut integral decays rapidly away from the branch point. Although the branch point contribution plays an important role in the half-space problem, the branch point singularity can be omitted when the bottom layer satisfies the high-contrast and lossy condition. Because the branch point is far away from the saddle point, only the pole contribution has to be considered [2,19,20].

The goal of this thesis is to develop the new asymptotic second-order formulas for the far-field components radiating from a vertical (VED) and horizontal electric dipole (HED) above an ordinary or plasmonic half-space medium by using the MSP method. The electromagnetic field components can be obtained either from the differentiation of the approximated expression of the Hertz potential or directly from the Sommerfeld integral form of each field component. In the VED problem, the asymptotic formula of Hertz potential is derived by using the MSP method [23]. It is noted that the higher-order terms from the differentiation of the error function in the Hertz potential are kept in the field components [43]. The Hertz potential can also be approximated by different methods. In Nazari and Huang [42], the geometric terms of Hertz potentials are approximated on the real-axis by the hyperbolic functions. In the plasmonic half-space model, the surface field formula is obtained using the vertical branch cut integral [19]. Their work is extended to the second-order expressions with limitation that the observation point is near the surface [20]. The HED problem is more complicated than the VED problem since more field components are involved. The advantage of using elevated HED transmitter and receiver over VED in the high

frequency (HF) band is reported in [22]. Moreover, we have found that it is required to use the second-order asymptotic formulation in computing the surface field, since the first-order formulation can obtain the null for some field components.

This thesis is organized as follows. In Chapter 2, the first-order and second-order approximation formulas for two variants of the MSP method for the field components of VED are derived. The numerical results from the second-order subtractive method are compared with the exact Sommerfeld integral results and Norton-Bannister formulas and have high accuracy in both ordinary and plasmonic cases. In Chapter 3, the field components of HED are derived by the second-order subtractive method. The numerical results from the second-order approximation are also compared with Norton-Bannister and King formulas and still demonstrate higher accuracy. The thesis ends with the conclusion and future works in Chapter 4.

CHAPTER II

VERTICL HERTZIAN DIPOLE OVER AN IMPERFECTLY CONDUCTING HALF SPACE*

2.1 Problem Statement and Formal Solution

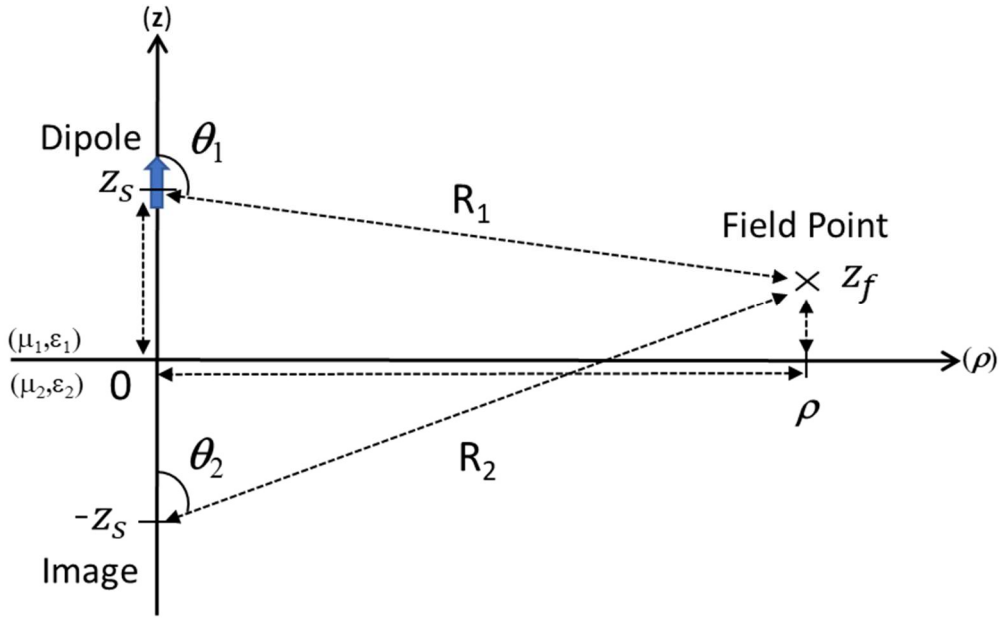

Figure 2.1: Vertical Hertzian Dipole in the top layer (air) at z_s above the conducting half space and field point is in the top layer.

Here we consider the half space problem, a unit strength vertical dipole (VED) source is on the z axis in the cylindrical coordinate system (ρ ,θ , z). The VED is at a height z_s away from the interface between medium 1 and medium 2 and the field point is located at (ρ, z_f), shown in Figure 2.1. The electromagnetic field components generated by the VED source can be obtained at any point in medium 1 and medium 2 can be known by solving the Sommerfeld formula. The medium on top is air and the bottom layer medium is an imperfect conductor which can be

*Reprinted with permission from "On the far-zone electromagnetic field of a vertical Hertzian dipole over an imperfectly conducting half-space with extensions to plasmonics" by K. A. Michalski and H.-I. Lin, 2017. Radio Science, vol. 52, no. 7, pp. 798-810, Copyright 2021 by John Wiley and Sons.

characterized by the dielectric function $\varepsilon_r = \varepsilon_r' + j\varepsilon_r''$ and the time convention $e^{-j\omega t}$ is implied. The passive medium is considered but may be ordinary medium ($\varepsilon_r'>0$) or plasmonic medium($\varepsilon_r'<0$).

The electromagnetic field expressions generated from a VED on top layer are shown below [20]:

$$E_z = -j\frac{\eta_1 {k_1}^2}{4\pi}\left[E_z^{(1)} - E_z^{(2)} + P_z\right], \tag{2.1}$$

$$E_\rho = -j\frac{\eta_1 {k_1}^2}{4\pi}\left[E_\rho^{(1)} + E_\rho^{(2)} + P_\rho\right], \tag{2.2}$$

$$H_\phi = -j\frac{{k_1}^2}{4\pi}\left[E_\phi^{(1)} - E_\phi^{(2)} + P_\phi\right]. \tag{2.3}$$

where η_1 is the intrinsic impedance and k_1 is the wave number in the medium1. The geometrical terms for each field component may be expressed as

$$E_z^{(i)} = [\sin^2\theta_i - (1 - 3\cos^2\theta_i)\left(\frac{j}{\Omega_i} + \frac{1}{{\Omega_i}^2}\right)]\frac{e^{-j\Omega_i}}{\Omega_i}, \tag{2.4}$$

$$E_\rho^{(i)} = -\sin\theta_i\cos\theta_i[1 - 3\left(\frac{j}{\Omega_i} + \frac{1}{{\Omega_i}^2}\right)]\frac{e^{-j\Omega_i}}{\Omega_i}, \tag{2.5}$$

$$E_\phi^{(i)} = \sin\theta_i\left(1 - \frac{j}{\Omega_i}\right)\frac{e^{-j\Omega_i}}{\Omega_i}, \tag{2.6}$$

with $\Omega_i = k_1 r_i$, and the Sommerfeld integrals

$$P_z = \int_{-\infty}^{\infty} \frac{1 - \overleftarrow{\Gamma_1^e}}{2jk_{z1}} e^{-jk_{z1}(z_f + z_s)} {H_0}^{(2)}(k_\rho\rho)(\frac{k_\rho}{k_1})^3 dk_\rho \tag{2.7}$$

$$P_\rho = \int_{-\infty}^{\infty} -\frac{1 + \overleftarrow{\Gamma_1^e}}{2} e^{-jk_{z1}(z_f + z_s)} {H_1}^{(2)}(k_\rho\rho)(\frac{k_\rho}{k_1})^2 \frac{dk_\rho}{k_1} \tag{2.8}$$

$$P_\phi = \int_{-\infty}^{\infty} -\frac{1 - \overleftarrow{\Gamma_1^e}}{2k_{z1}} e^{-jk_{z1}(z_f + z_s)} {H_1}^{(2)}(k_\rho\rho)(\frac{k_\rho}{k_1})^2 dk_\rho \tag{2.9}$$

with

$$\overleftarrow{\Gamma_1^e} = \frac{\frac{k_{z2}}{\epsilon_r} - k_{z1}}{\frac{k_{z2}}{\epsilon_r} + k_{z1}}, \tag{2.10}$$

$$k_{\mathrm{zi}} = \sqrt{{k_i}^2 - {k_\rho}^2}\ , \text{ i is the index for the medium} \tag{2.11}$$

Where $H_n^{(2)}$ is the Hankel function of the second kind and order n and $\overleftarrow{\Gamma_1^e}$ is the reflection coefficient for the transverse-magnetic wave. The closed form expressions in (2.4) - (2.6) are the direct contributions from dipole and its image. The Sommerfeld integrals in (2.7) - (2.9) represent the correction of the imperfect conducting bottom layer.

To evaluate the Sommerfeld integrals in (2.7) - (2.9) in complex k_ρ-plane, the singularities are needed to be located first. The branch points come from the square root in k_{z1} and k_{z2} and its associated branch cuts are in the second and fourth quadrants in the complex k_ρ-plane. The pole location, the root of the denominator in (2.10), is at

$$k_p = \sqrt{\frac{\epsilon_r}{1+\epsilon_r}}\, k_1. \tag{2.12}$$

The integration path C and the singularities above are on the top sheet of the four sheeted Riemann sheets, which is defined by Im $k_{z1}<0$ and Im $k_{z2}<0$.

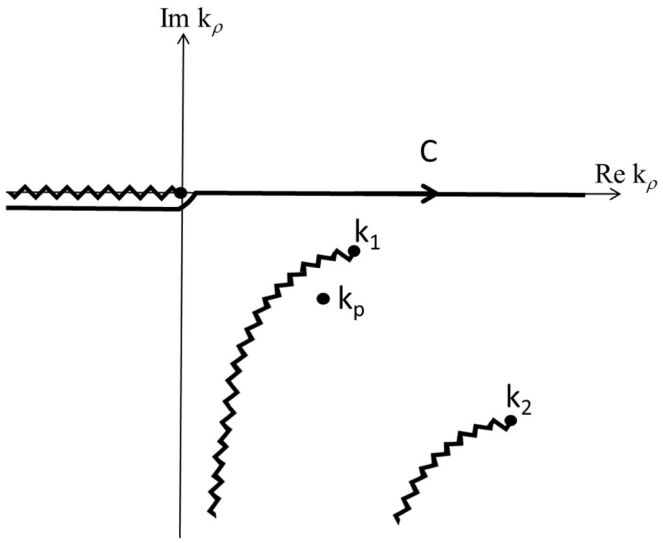

Figure 2.2: The illustration plot for the integration path C in the k_ρ-plane and the singularities in the fourth-quadrant.

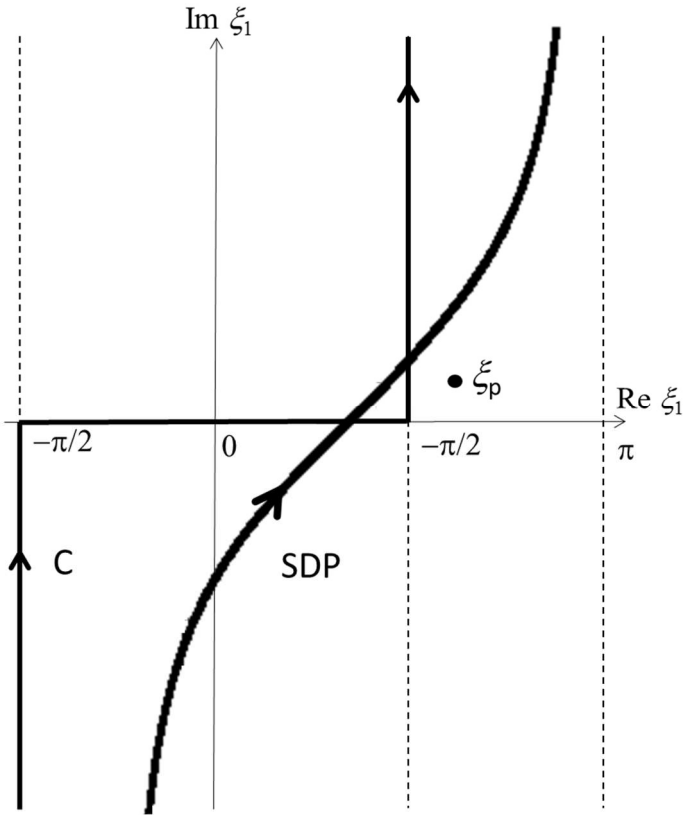

Figure 2.3: The integration C and SDP are illustrated in the ξ_1-plane.

2.2 Angular Transformation

To facilitate the approximation of the Sommerfeld integrals, the transformation

$$k_\rho = k_1 \sin \xi_1,\ k_{z1} = k_1 \cos \xi_1, \tag{2.13}$$

is used to transform the integration path C from complex k_ρ-plane in Figure (2.2) to the angular spectrum ξ_1-plane in Figure (2.3), and use the substitution

$$\rho = r_2 \sin\theta_2\ ,\ \ z_f + z_s = r_2 \cos\theta_2, \tag{2.14}$$

the Sommerfeld integrals in (2.7) - (2.9) can be expressed as

$$P_\alpha = \frac{1}{\sqrt{2\pi j \Omega_2}} \int_C g_\alpha(\xi_1) e^{-j\Omega_2 \cos(\xi_1 - \theta_2)} d\xi_1 \tag{2.15}$$

where α is the direction of field components: z, ρ or ϕ, the integrands can be expressed as

$$g_z(\xi_1) = \left[1 + \Gamma_{||}(\xi_1)\right]\sin^2\xi_1 \sqrt{\frac{\sin\xi_1}{\sin\theta_2}} H_0(\Omega_2 \sin\theta_2 \sin\xi_1), \tag{2.16}$$

$$g_\rho(\xi_1) = \left[1 - \Gamma_{||}(\xi_1)\right]\cos\xi_1 \sin\xi_1 \sqrt{\frac{\sin\xi_1}{\sin\theta_2}} H_1(\Omega_2 \sin\theta_2 \sin\xi_1), \tag{2.17}$$

$$g_\phi(\xi_1) = \left[1 + \Gamma_{||}(\xi_1)\right]\sin\xi_1 \sqrt{\frac{\sin\xi_1}{\sin\theta_2}} H_1(\Omega_2 \sin\theta_2 \sin\xi_1), \tag{2.18}$$

with

$$\Gamma_{||}(\xi_1) = \frac{\cos\xi_1 - \dfrac{\delta(\xi_1)}{\epsilon_r}}{\cos\xi_1 + \dfrac{\delta(\xi_1)}{\epsilon_r}}, \quad \delta(\xi_1) = \sqrt{\epsilon_r - \sin^2\xi_1} \tag{2.19}$$

and the normalized Hankel function [16] is introduced

$$H_n(z) = j^{-n}\sqrt{\frac{\pi z}{2j}} H_n{}^{(2)}(z) e^{jz} \sim 1 - j\frac{(4n^2 - 1)}{8z} + O(z^{-2}). \tag{2.20}$$

The mapping of pole in k_ρ-plane (12) to ξ_1-plane is located at ξ_{1p}, which satisfies

$$\sin\xi_{1p} = \sqrt{\frac{\epsilon_r}{\epsilon_r + 1}}, \qquad \cos\xi_{1p} = -\sqrt{\frac{1}{\epsilon_r + 1}}. \tag{2.21}$$

2.3 Application of the Modified Saddle Point method

The transformed Sommerfeld integrals in (2.15) can be approximated by the modified saddle point (MSP) method with two variants- subtractive method and multiplicative method- are given in the Appendix A. The first order and second order approximations of the Sommerfeld integrals in (2.15) for subtractive and multiplicative variants are listed in the following section.

2.3.1 Subtractive Method

2.3.1.1 First Order Approximation

By applying (A15), we have

$$P_z \sim \sin^2\theta_2 (1+\Gamma_{||}) \frac{e^{-j\Omega_2}}{\Omega_2} + \sin\xi_{1p} Q_p \mathcal{F}(p) \frac{e^{-j\Omega_2}}{\Omega_2}, \tag{2.22}$$

$$P_\rho \sim \cos\theta_2 \sin\theta_2 (1+\Gamma_{||}) \frac{e^{-j\Omega_2}}{\Omega_2} - \cos\xi_{1p} Q_p \mathcal{F}(p) \frac{e^{-j\Omega_2}}{\Omega_2}, \tag{2.23}$$

$$P_\phi \sim \sin\theta_2 (1+\Gamma_{||}) \frac{e^{-j\Omega_2}}{\Omega_2} + Q_p \mathcal{F}(p) \frac{e^{-j\Omega_2}}{\Omega_2}, \tag{2.24}$$

where

$$Q_p = -\frac{2{\epsilon_r}^2}{{\epsilon_r}^2 - 1} \frac{\cos\xi_{1p}}{\sqrt{2j} s_p} \sqrt{\frac{\sin\xi_{1p}}{\sin\theta_2}}. \tag{2.25}$$

For the surface to surface propagation case, where z_f=z_s=0, the formula (22)-(24) reduce to

$$P_z \sim \sin\xi_{1p} Q_p \mathcal{F}(p) \frac{e^{-j\Omega_2}}{\Omega_2}, \tag{2.26}$$

$$P_\rho \sim -\cos\xi_{1p} Q_p \mathcal{F}(p) \frac{e^{-j\Omega_2}}{\Omega_2}, \tag{2.27}$$

$$P_\phi \sim Q_p \mathcal{F}(p) \frac{e^{-j\Omega_2}}{\Omega_2}. \tag{2.28}$$

The wave tilt at the surface [15,21] can be predicted as

$$\frac{P_\rho}{P_z} \sim \frac{1}{\sqrt{\epsilon_r}} \tag{2.29}$$

2.3.1.2 Second Order Approximation

By applying (A16), we have

$$P_z \sim \sin^2\theta_2\left(1+\Gamma_{||}\right)\frac{e^{-j\Omega_2}}{\Omega_2} - j\left\{\begin{array}{c}(1-3\cos^2\theta_2)\left(1+\Gamma_{||}\right)\\ +\sin\theta_2\left(1-\Gamma_{||}\right)S\left[3\cos\theta_2\left(1+\frac{\sin^2\theta_2}{2\delta^2}\right)+\sin\theta_2 S\right]\end{array}\right\}\frac{e^{-j\Omega_2}}{{\Omega_2}^2} + \sin\xi_{1p}Q_p[\mathcal{F}(p)+\frac{1}{2p}]\frac{e^{-j\Omega_2}}{\Omega_2}, \tag{2.30}$$

$$P_\rho \sim \cos\theta_2\sin\theta_2\left(1-\Gamma_{||}\right)\frac{e^{-j\Omega_2}}{\Omega_2} - j\left\{\begin{array}{c}3\cos\theta_2\sin\theta_2\left(1-\Gamma_{||}\right)\\ +\left(1-\Gamma_{||}\right)S\left[1-3\cos^2\theta_2\left(1+\frac{\sin^2\theta_2}{2\delta^2}\right)-\cos\theta_2\sin\theta_2 S\right]\end{array}\right\}\frac{e^{-j\Omega_2}}{{\Omega_2}^2} - \cos\xi_{1p}Q_p[\mathcal{F}(p)+\frac{1}{2p}]\frac{e^{-j\Omega_2}}{\Omega_2}, \tag{2.31}$$

$$P_\phi \sim \sin\theta_2\left(1+\Gamma_{||}\right)\frac{e^{-j\Omega_2}}{\Omega_2} - j\left\{\begin{array}{c}\sin\theta_2\left(1+\Gamma_{||}\right)\\ +\left(1-\Gamma_{||}\right)S\left[2\cos\theta_2\left(1+\frac{3\sin^2\theta_2}{4\delta^2}\right)+\sin\theta_2 S\right]\end{array}\right\}\frac{e^{-j\Omega_2}}{{\Omega_2}^2} + Q_p[\mathcal{F}(p)+\frac{1}{2p}]\frac{e^{-j\Omega_2}}{\Omega_2}, \tag{2.32}$$

where

$$S = \sin\theta_2\frac{\epsilon_r(\epsilon_r-1)}{2\delta^3}(1-\Gamma_{||}). \tag{2.33}$$

For the surface-to-surface propagation case, where z_f=z_s=0, the formula (30)-(32) reduce to

$$P_z \sim -j\frac{2{\epsilon_r}^2}{\epsilon_r-1}\frac{e^{-j\Omega_2}}{{\Omega_2}^2} + \sin\xi_{1p}Q_p[\mathcal{F}(p)+\frac{1}{2p}]\frac{e^{-j\Omega_2}}{\Omega_2}, \tag{2.34}$$

$$P_\rho \sim -j\frac{2\epsilon_r}{\sqrt{\epsilon_r-1}}\frac{e^{-j\Omega_2}}{{\Omega_2}^2} - \cos\xi_{1p}Q_p[\mathcal{F}(p)+\frac{1}{2p}]\frac{e^{-j\Omega_2}}{\Omega_2}, \tag{2.35}$$

$$P_\phi \sim -j\frac{2{\epsilon_r}^2}{\epsilon_r-1}\frac{e^{-j\Omega_2}}{{\Omega_2}^2} + Q_p[\mathcal{F}(p)+\frac{1}{2p}]\frac{e^{-j\Omega_2}}{\Omega_2}. \tag{2.36}$$

2.3.2 Multiplicative Method

2.3.2.1 First Order Approximation

By applying (A25), we have

$$P_z \sim \sin^2\theta_2\left(1+\Gamma_{||}\right)\frac{e^{-j\Omega_2}}{\Omega_2} - \sqrt{2j}s_p\sin\theta_2\left[\frac{5}{2}\cos\theta_2(1+\Gamma_{||}) - \sin\theta_2(1-\Gamma_{||})S\right]\mathcal{F}(p)\frac{e^{-j\Omega_2}}{\Omega_2}, \tag{2.37}$$

$$P_\rho \sim \cos\theta_2\sin\theta_2\left(1-\Gamma_{||}\right)\frac{e^{-j\Omega_2}}{\Omega_2} + \sqrt{2j}s_p(1-\Gamma_{||})\left(1-\frac{5}{2}\cos^2\theta_2 - \cos\theta_2\sin\theta_2 S\right)\mathcal{F}(p)\frac{e^{-j\Omega_2}}{\Omega_2}, \tag{2.38}$$

$$P_\phi \sim \sin\theta_2\left(1+\Gamma_{||}\right)\frac{e^{-j\Omega_2}}{\Omega_2} - \sqrt{2j}s_p\left[\frac{3}{2}\cos\theta_2(1+\Gamma_{||}) - \sin\theta_2(1-\Gamma_{||})S\right]\mathcal{F}(p)\frac{e^{-j\Omega_2}}{\Omega_2}. \tag{2.39}$$

For the surface to surface propagation case, where z_f=z_s=0, the formula (30)-(32) reduce to

$$P_z \sim \sqrt{2j}s_p\frac{2\epsilon_r}{\sqrt{\epsilon_r-1}}\mathcal{F}(p)\frac{e^{-j\Omega_2}}{\Omega_2}, \tag{2.40}$$

$$P_\rho \sim \sqrt{2j}s_p 2\mathcal{F}(p)\frac{e^{-j\Omega_2}}{\Omega_2}, \tag{2.41}$$

$$P_\phi \sim \sqrt{2j}s_p\frac{2\epsilon_r}{\sqrt{\epsilon_r-1}}\mathcal{F}(p)\frac{e^{-j\Omega_2}}{\Omega_2}. \tag{2.42}$$

2.3.2.2 Second Order Approximation

By applying (A26), we have

$$P_z \sim \sin^2\theta_2\left(1+\Gamma_{||}\right)\frac{e^{-j\Omega_2}}{\Omega_2} + 2js_p{}^2\{\frac{3}{8}(3-8\cos^2\theta_2)(1+\Gamma_{||}) + \sin\theta_2(1-\Gamma_{||})S[3\cos\theta_2(1+\frac{\sin^2\theta_2}{2\delta^2}) + \sin\theta_2 S]\}\mathcal{F}(p)\frac{e^{-j\Omega_2}}{\Omega_2}, \tag{2.43}$$

$$P_\rho \sim \cos\theta_2\sin\theta_2(1-\Gamma_{||})\frac{e^{-j\Omega_2}}{\Omega_2} - 2js_p{}^2\{\frac{3}{8}(1-8\sin^2\theta_2)(1-\Gamma_{||}) - (1-\Gamma_{||})S[1-3\cos^2\theta_2(1+\frac{\sin^2\theta_2}{2\delta^2}) - \cos\theta_2\sin\theta_2 S]\}\mathcal{F}(p)\frac{e^{-j\Omega_2}}{\Omega_2}, \tag{2.44}$$

$$P_\phi \sim \sin\theta_2(1+\Gamma_{||})\frac{e^{-j\Omega_2}}{\Omega_2} - 2js_p{}^2\{(\frac{3}{8\sin\theta_2} - \sin\theta_2)(1+\Gamma_{||}) - (1-\Gamma_{||})S[2\cos\theta_2(1+\frac{3\sin^2\theta_2}{4\delta^2}) + \sin\theta_2 S]\}\mathcal{F}(p)\frac{e^{-j\Omega_2}}{\Omega_2}. \tag{2.45}$$

For the surface-to-surface propagation case, where z_f=z_s=0, the formula (30)-(32) reduce to

$$P_z \sim 2js_p{}^2\frac{2\epsilon_r{}^2}{\epsilon_r-1}\mathcal{F}(p)\frac{e^{-j\Omega_2}}{\Omega_2}, \tag{2.46}$$

$$P_\rho \sim 2js_p{}^2\frac{2\epsilon_r}{\sqrt{\epsilon_r-1}}\mathcal{F}(p)\frac{e^{-j\Omega_2}}{\Omega_2}, \tag{2.47}$$

$$P_\phi \sim 2js_p{}^2\frac{2\epsilon_r{}^2}{\epsilon_r-1}\mathcal{F}(p)\frac{e^{-j\Omega_2}}{\Omega_2}. \tag{2.48}$$

2.4 Numerical Results

Table 2.1: Model considered for the ordinary(left) and plasmonic(right) medium.

	Seawater @ f = 30 MHz	Gold @ λ_0=633nm
ε_r'	80	-
σ	4.0 S/m	-
ε_r	$80 - j\,2.39668 \times 10^{3}$	$-11.53015 - j\,1.20367$
k_p/k_0	$0.999993 - j\,2.08385 \times 10^{-4}$	$1.045833 - j\,5.12279 \times 10^{-3}$
$k_0\rho\|_{knee}$	4.8×10^{3}	23.2
z_s	10 m	100 nm

Seawater and gold problems listed in Table 2.1 are evaluated by the asymptotic formulas compared with the exact Sommerfeld integral results in this section. The sea water problem is the example for the ordinary medium [22] and the gold problem is the example for plasmonic medium. The seawater problem is considered as high-contrast, but the gold problem is only marginally satisfied. Therefore, when the field point is near the interface, the pole is very close to the saddle point in the k_ρ-plane. In this case, the modified saddle point method should be applied. Using (2.12), we can observed that the pole is on the left of k_0 for seawater which contributes the Zenneck surface wave on the interface. For gold case, the pole is on the right of k_0, which contributes the surface plasmon polariton [23]. The first- and second-order MSP approximations for two variants are computed in the following tables and plots. Sub1 and Sub2 stands for the first- and second-order subtractive variants of the MSP method. Mul1 and Mul2 represents the first- and second-order multiplicative variants. The results from Norton-Banmister formulation [5] is denoted as Nort.

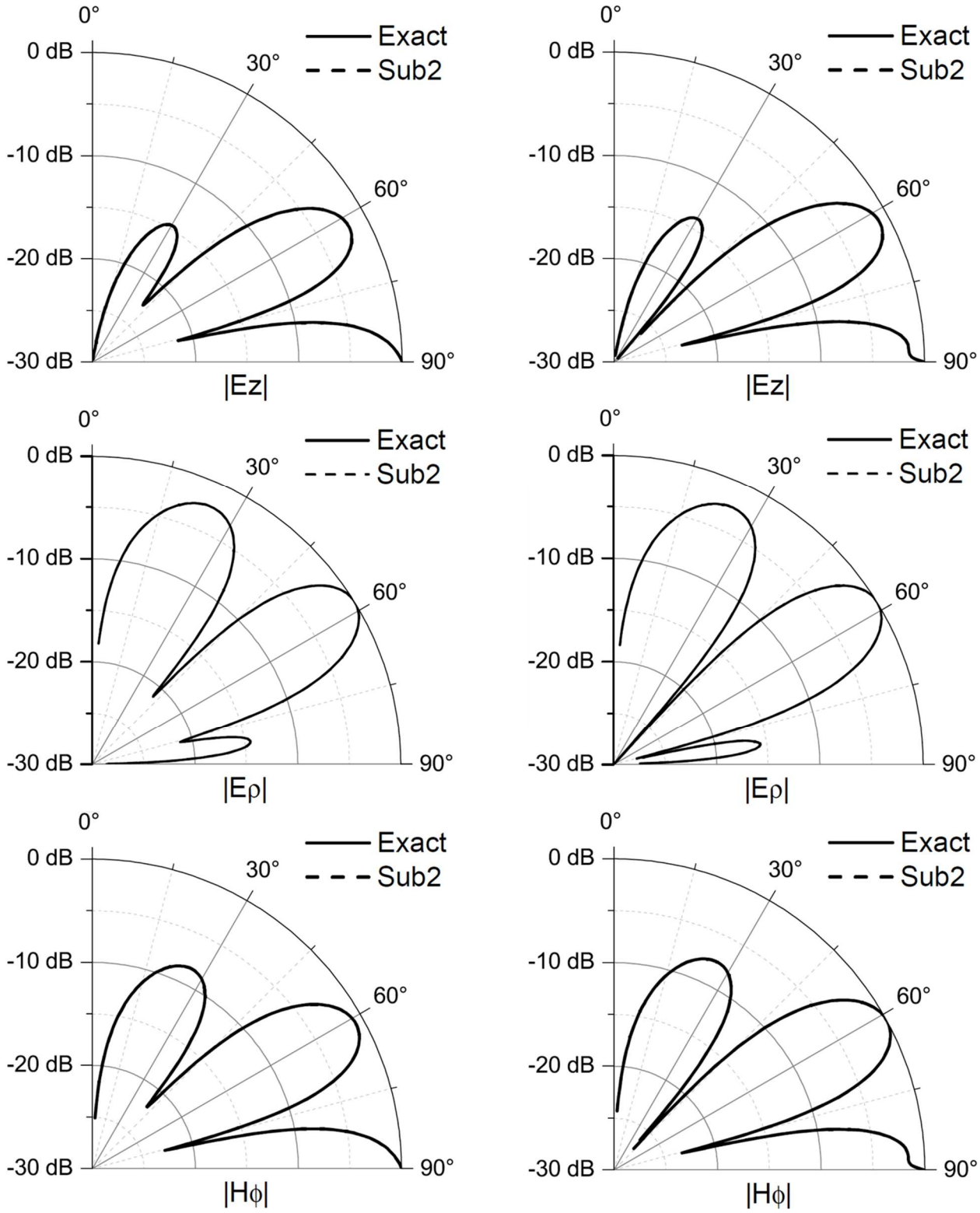

$k_0r = 100$ $k_0r = 1000$

Figure 2.4: The normalized field patterns for the seawater case at k_0r=100 and k_0r=1000.

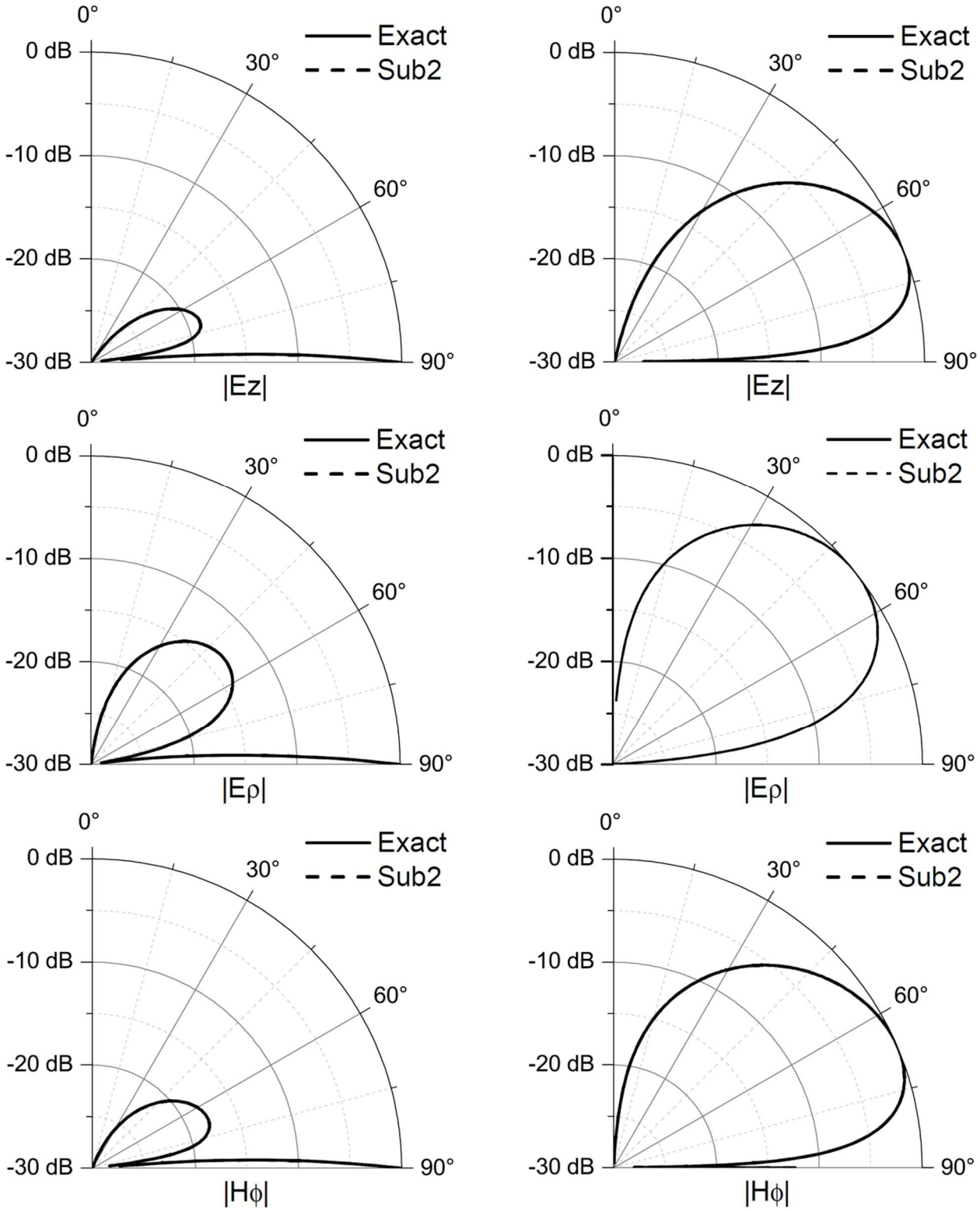

$k_0r = 100$ $k_0r = 1000$

Figure 2.5: The normalized field patterns for the gold case at k_0r=100 and k_0r=1000.

Table 2.2: RMS Errors (%) in field patterns at k_0r = 100 for the seawater problem.

	Sub1	Sub2	Mul1	Mul2	Nort
E_z	5.6	5.3×10^{-2}	7.4	0.9	0.4
E_ρ	0.3	8.1×10^{-3}	0.5	0.2	1.1×10^{-2}
H_ϕ	3.1	1.1×10^{-2}	8.5	2.4	0.1

Table 2.3: RMS Errors (%) in field patterns at k_0r = 1000 for the seawater problem.

	Sub1	Sub2	Mul1	Mul2	Nort
E_z	3.0	3.0×10^{-3}	2.7	0.2	8.7×10^{-2}
E_ρ	5.2×10^{-2}	4.5×10^{-3}	0.1	4.6×10^{-2}	4.6×10^{-3}
H_ϕ	0.5	2.2×10^{-3}	1.4	0.7	2.1×10^{-2}

Table 2.4: RMS Errors (%) in field patterns at k_0r = 100 for the gold problem.

	Sub1	Sub2	Mul1	Mul2	Nort
E_z	13.0	0.2	12.0	9.5	18.0
E_ρ	1.8	0.1	4.6	2.3	6.4
H_ϕ	3.1	0.3	8.5	5.7	14.0

Table 2.5: RMS Errors (%) in field patterns at k_0r = 1000 for the gold problem.

	Sub1	Sub2	Mul1	Mul2	Nort
E_z	9.9	1.0×10^{-2}	8.1	0.9	5.1
E_ρ	1.4	7.9×10^{-3}	0.9	0.8	5.5
H_ϕ	0.4	2.9×10^{-3}	1.2	1.9	4.3

For the two problems in Table 2.1, the normalized field patterns are plotted in Figure 2.4 and Figure 2.5 from $\theta_2 = 3$ (near the z axis) to $\theta_2 = 90$ (on the interface) are computed by rigorous numerical integration of Sommerfeld integrals [24,25] (solid line) and by Sub2 (dashed line) for two radii k_0r=100 and 1000. Although the Exact and Sub2 results are visually indistinguishable in the field pattern plots, they are not identical. In Figure 2.4, $|E_z|$ and $|H_\phi|$ has maximus values on the interface, like fields above perfect conductor, is because seawater in 30 MHz behaves as a good

conductor. In the plasmonic case of Figure 2.5, a strong field contributes from SPP is on the interface at k_0r =100. But at k_0r =1000, the strong field disappears due to the exponential decay factor in the attenuation function annihilates the contribution term for the SPP. The relative root-mean-square (RMS) errors for plotted field patterns are listed in Table 2.2 to 2.5. Note that the RMS errors were only computed in the range $k_0r_2\sin^2\theta_2>10$. The Sub2 method is still more accurate than Sub1.

Table 2.6: RMS Errors (%) in the surface field for the seawater problem

	Sub1	Sub2	Mul1	Mul2	Nort
E_z	0.3	2.4×10^{-2}	0.3	0.3	4.6×10^{-2}
E_ρ	0.2	7.6×10^{-3}	0.3	0.3	5.5×10^{-2}
H_ϕ	0.2	7.6×10^{-3}	0.3	0.2	3.8×10^{-2}

Table 2.7: RMS Errors (%) in the surface field for the gold problem

	Sub1	Sub2	Mul1	Mul2	Nort
E_z	15.0	1.5×10^{-2}	11.0	11.1	85.0
E_ρ	11.3	3.6×10^{-3}	8.4	8.4	111.0
H_ϕ	10.9	3.8×10^{-3}	8.1	8.1	121.0

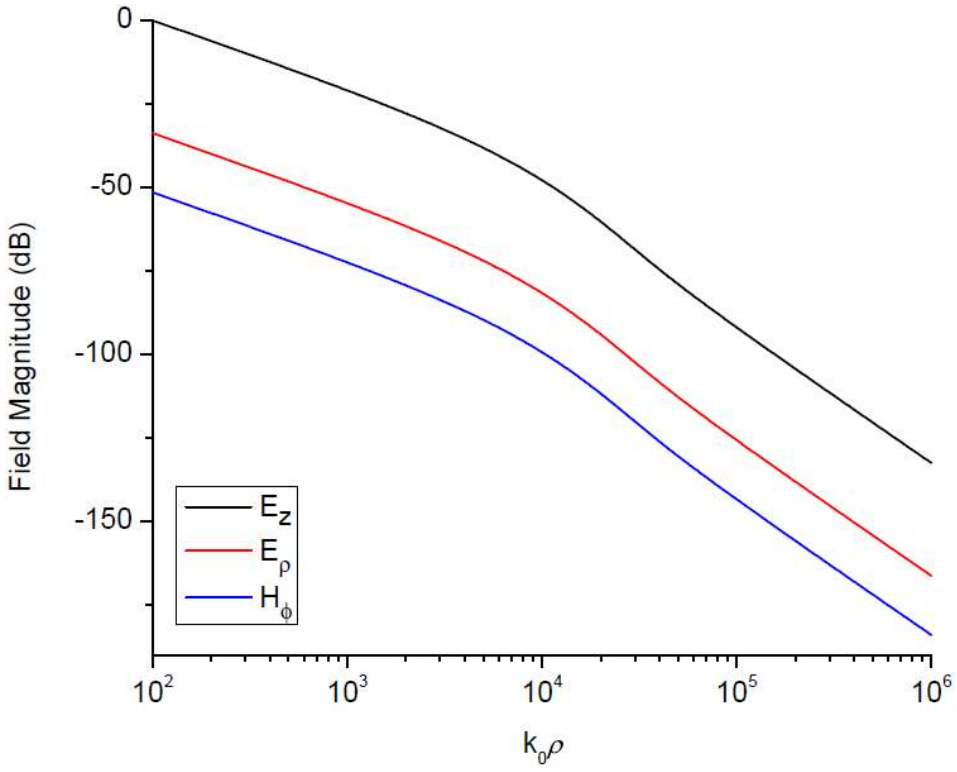

Figure 2.6: Surface fields for the seawater case computed by Sub2.

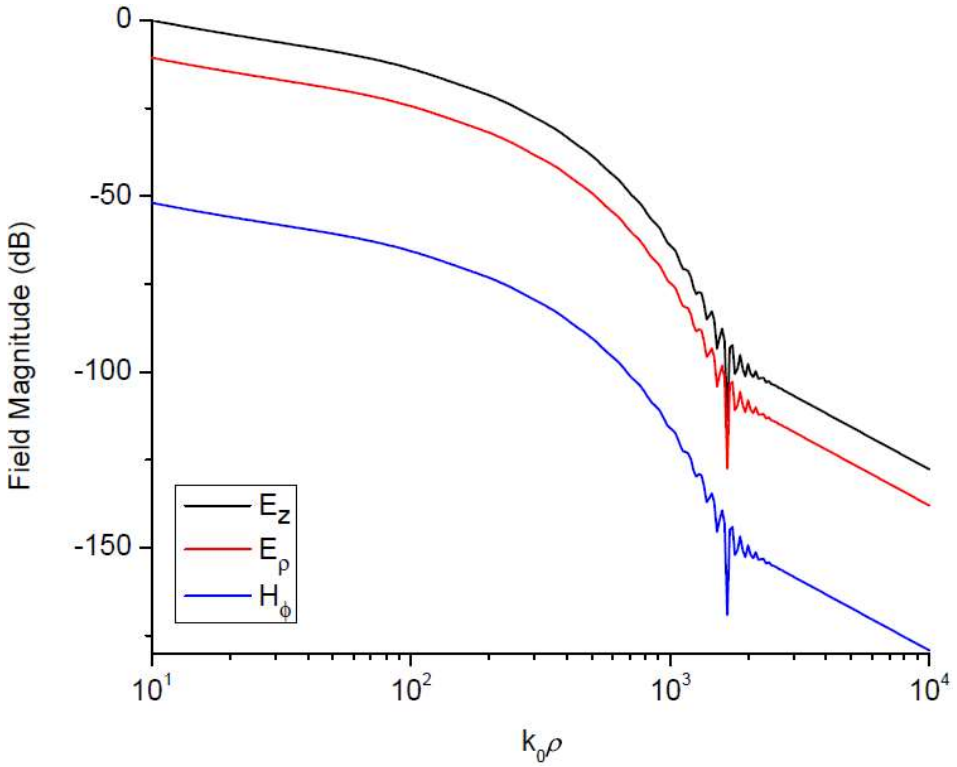

Figure 2.7: Surface fields for the seawater case computed by Sub2.

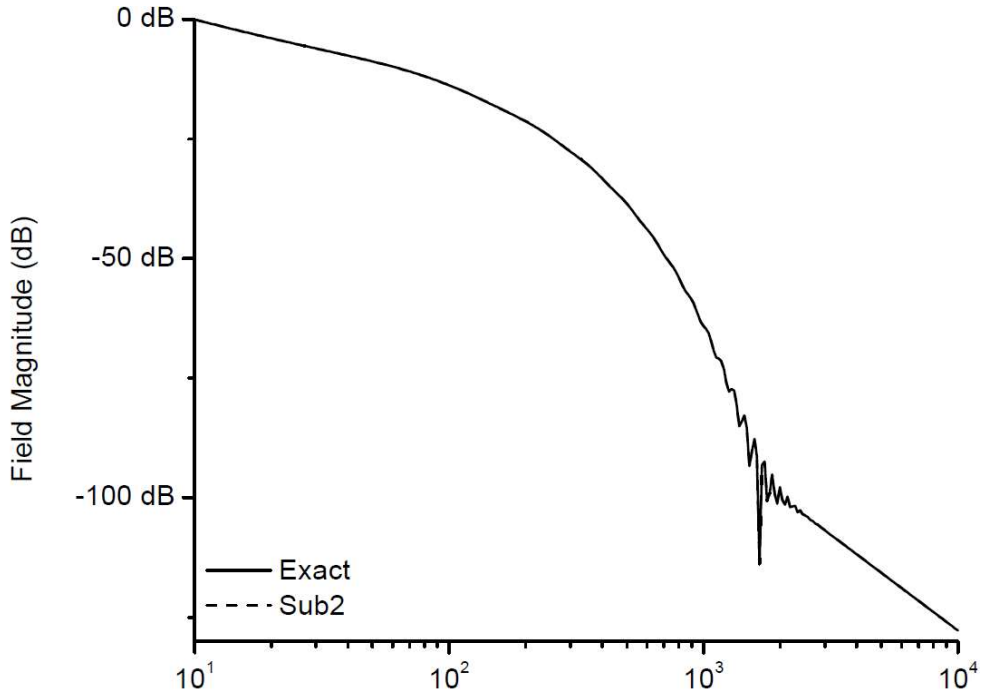

(a)

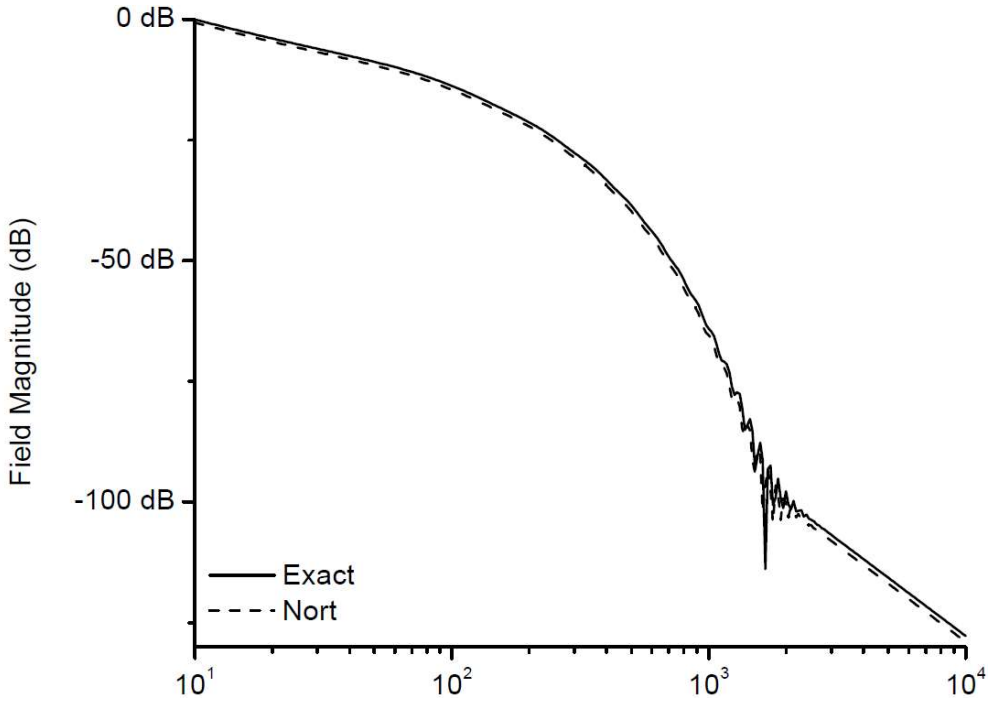

(b)

Figure 2.8: Normalized $|E_z|$ surface fields for the gold case computed by (a)Sub2 and (b)Nort, and compared with the exact results.

In Figures 2.6 and 2.7, the magnitude of the surface fields computed by Sub2 are plotted for the two problems, which are normalized by the maximum field magnitude. In the seawater case, the dB scale plot covers the four-decade range from $10<k_0\rho<10^4$. Three-decade range are covered from $10^2< k_0\rho <10^6$ in the gold case. Note that the transition between the $1/\rho$ and $1/\rho^2$ occurs near the knee point when the numerical distance is equal to 1. The knee point can be used to estimate the slope changed in Figure 2.6 in the seawater case, but fails on the gold case. The reason is the asymptotic behavior for the gold case changes from 1/sqrt(ρ) to $1/\rho^2$ with increasing $k_0\rho$ and it is not the transition for knee point to predict. The RMS percent errors for the seawater and gold problems for computing the surface fields are listed in Tables 2.6 and 2.7. We can see that Sub2 performs better than other method, especially in the gold case, where the RMS errors of Nort are surprisingly large. This phenomenon can be observed by plotting the surface field by comparing the results from two different methods- Sub2 and Nort - with exact Sommerfeld integral results in Figure 2.8 and Nort results are visibly shifted to the exact. This small shit results in the large amount of errors in Nort.

CHAPTER III

HORIZONTAL ELECTRIC DIPOLE OVER AN IMPERFECTLY CONDUCTING HALF SPACE*

3.1 Problem Statement and Formal Solution

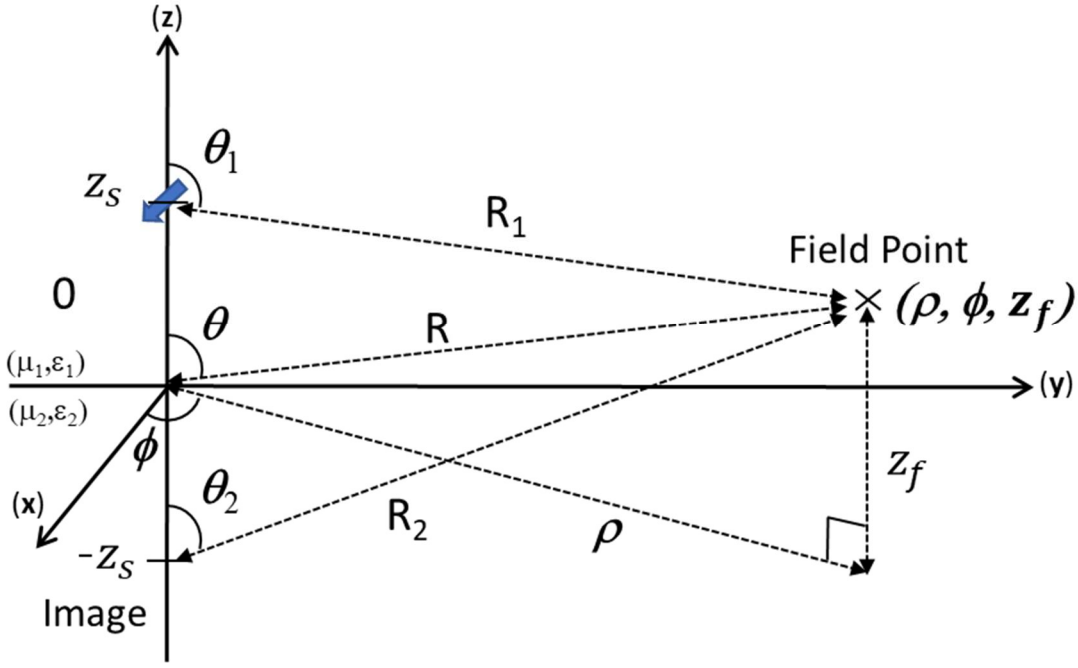

Figure 3.1: Horizontal Electric Dipole along the x-axis in the top layer (air) at z_s above the conducting half space and field point is in the top layer.

In Figure 3.1, a unit strength, x-oriented, horizontal dipole source is at a height z_s on the z axis away from the interface between medium 1 and medium 2. The field point to determine the far-zone electromagnetic fields above or on the interface ($z \geq 0$) is located at (ρ, ϕ, z_f). The medium

*Reprinted with permission from "On the far-zone electromagnetic field of a horizontal electric dipole over an imperfectly conducting half-space with extensions to plasmonics" by K. A. Michalski and H.-I. Lin, 2018. Radio Science, vol. 53, no. 1, pp. 62-82, Copyright 2021 by John Wiley and Sons.

on top is air and the bottom layer medium is an imperfect conductor which can be characterized by the dielectric function $\varepsilon_r = \varepsilon_r' + j\varepsilon_r''$ and the time convention $e^{-j\omega t}$ is implied.

The electric field components generated from a HED on top layer are shown below [41]:

$$E_z = -\cos\phi \frac{j\eta_1 {k_1}^2}{4\pi}[E_z^{(1)} - E_z^{(2)} + E_z^s], \tag{3.1}$$

$$E_\rho = -\cos\phi \frac{j\eta_1 {k_1}^2}{4\pi}[E_\rho^{(1)} - E_\rho^{(2)} + E_\rho^s], \tag{3.2}$$

$$E_\phi = \sin\phi \frac{j\eta_1 {k_1}^2}{4\pi}[E_\phi^{(1)} - E_\phi^{(2)} + E_\phi^s]. \tag{3.3}$$

The closed-form geometrical terms for each field component may be expressed as

$$E_z^{(i)} = -\sin\theta_i \cos\theta_i [1 - 3(\frac{j}{\Omega_i} + \frac{1}{{\Omega_i}^2})] \frac{e^{-j\Omega_i}}{\Omega_i}, \tag{3.4}$$

$$E_\rho^{(i)} = [\cos^2\theta_i + (2 - 3\cos^2\theta_i)(\frac{j}{\Omega_i} + \frac{1}{{\Omega_i}^2})] \frac{e^{-j\Omega_i}}{\Omega_i}, \tag{3.5}$$

$$E_\phi^{(i)} = [1 - (\frac{j}{\Omega_i} + \frac{1}{{\Omega_i}^2})] \frac{e^{-j\Omega_i}}{\Omega_i}, \tag{3.6}$$

with $\Omega_i = k_1 r_i$. (i=1,2)

The Sommerfeld terms for electric field components

$$E_z^s = -P_1, \tag{3.7}$$

$$E_\rho^s = P_2 - \frac{j}{k_0\rho} P_3 + \frac{j}{k_0\rho} P_4, \tag{3.8}$$

$$E_\phi^s = P_5 + \frac{j}{k_0\rho} P_3 - \frac{j}{k_0\rho} P_4, \tag{3.9}$$

With

$$P_1 = -\int_0^\infty \left(1 + \overleftarrow{\Gamma_1^e}\right) e^{-jk_{z1}(z_f + z_s)} J_1(k_\rho \rho) \left(\frac{k_\rho}{k_0}\right)^2 \frac{dk_\rho}{k_0}, \tag{3.10}$$

$$P_2 = \int_0^\infty (1 + \overleftarrow{\Gamma_1^e}) \frac{e^{-jk_{z1}(z_f + z_s)}}{jk_{z1}} J_0(k_\rho \rho) \left(\frac{k_{z1}}{k_0}\right)^2 (\frac{k_\rho}{k_0}) dk_\rho, \tag{3.11}$$

$$P_3 = -\int_0^\infty (1 + \overleftarrow{\Gamma_1^e}) e^{-jk_{z1}(z_f + z_s)} J_1(k_\rho \rho) \frac{k_{z1}}{k_0} \frac{dk_\rho}{k_0}, \tag{3.12}$$

$$P_4 = -\int_0^\infty (1 + \overleftarrow{\Gamma_1^h}) \frac{e^{-jk_{z1}(z_f + z_s)}}{k_{z1}} J_1(k_\rho \rho) dk_\rho, \tag{3.13}$$

$$P_5 = \int_0^{\infty} (1 + \overleftarrow{\Gamma_1^h}) \frac{e^{-jk_{z1}(z_f+z_s)}}{j\, k_{z1}} J_0(k_\rho \rho) \frac{k_\rho}{k_0} dk_\rho, \tag{3.14}$$

The magnetic field components are expressed as:

$$H_z = \sin\phi \frac{jk_1{}^2}{4\pi} [H_z^{(1)} - H_z^{(2)} + H_z^s], \tag{3.15}$$

$$H_\rho = \sin\phi \frac{jk_1{}^2}{4\pi} [H_y^{(1)} - H_y^{(2)} + H_\rho^s], \tag{3.16}$$

$$H_\phi = \cos\phi \frac{jk_1{}^2}{4\pi} \left[H_y^{(1)} - H_y^{(2)} + H_\phi^s\right], \tag{3.17}$$

With the geometrical terms

$$H_z^{(i)} = \sin\theta_i [1 - \frac{j}{\Omega_i}] \frac{e^{-j\Omega_i}}{\Omega_i}, \tag{3.18}$$

$$H_y^{(i)} = -\cos\theta_i [1 - \frac{j}{\Omega_i}] \frac{e^{-j\Omega_i}}{\Omega_i}, \tag{3.19}$$

with $\Omega_i = k_1 r_i$, and the Sommerfeld terms

$$H_z^s = P_6, \tag{3.20}$$

$$H_\rho^s = -P_7 - \frac{j}{k_0 \rho} P_8 + \frac{j}{k_0 \rho} P_9, \tag{3.21}$$

$$H_\phi^s = -P_{10} + \frac{j}{k_0 \rho} P_8 - \frac{j}{k_0 \rho} P_9, \tag{3.22}$$

With

$$P_6 = -\int_0^{\infty} (1 + \overleftarrow{\Gamma_1^h}) \frac{e^{-jk_{z1}(z_f+z_s)}}{k_{z1}} J_1(k_\rho \rho) \left(\frac{k_\rho}{k_0}\right)^2 dk_\rho, \tag{3.23}$$

$$P_7 = -j \int_0^{\infty} (1 + \overleftarrow{\Gamma_1^h}) e^{-jk_{z1}(z_f+z_s)} J_0(k_\rho \rho) \frac{k_\rho}{k_0} \frac{dk_\rho}{k_0}, \tag{3.24}$$

$$P_8 = -\int_0^{\infty} (1 + \overleftarrow{\Gamma_1^e}) e^{-jk_{z1}(z_f+z_s)} J_1(k_\rho \rho) \frac{dk_\rho}{k_0}, \tag{3.25}$$

$$P_9 = -\int_0^{\infty} (1 + \overleftarrow{\Gamma_1^h}) e^{-jk_{z1}(z_f+z_s)} J_1(k_\rho \rho) \frac{dk_\rho}{k_0}, \tag{3.26}$$

$$P_{10} = -j \int_0^{\infty} (1 + \overleftarrow{\Gamma_1^e}) e^{-jk_{z1}(z_f+z_s)} J_0(k_\rho \rho) \frac{k_\rho}{k_0} \frac{dk_\rho}{k_0}. \tag{3.27}$$

Where

$$\overleftarrow{\Gamma_1^e} = \frac{\frac{k_{z2}}{\epsilon_r} - k_{z1}}{\frac{k_{z2}}{\epsilon_r} + k_{z1}}, \tag{3.28}$$

$$\overleftarrow{\Gamma_1^h} = \frac{k_{z1} - k_{z2}}{k_{z1} + k_{z2}}, \tag{3.29}$$

$k_{zi} = \sqrt{{k_i}^2 - {k_\rho}^2}$, i is the index for the medium. (3.30)

Jn with n=0,1 is the Bessel function of order n and Γ_1^e and Γ_1^h is the reflection coefficient for transverse-electric and transverse-magnetic wave. The pole location, the root of the denominator in (3.28), is at

$$k_p = \sqrt{\frac{\epsilon_r}{1+\epsilon_r}}k_1. \tag{3.31}$$

3.2 Angular Transformation

To facilitate the approximation of the Sommerfeld integrals, the transformation

$$k_\rho = k_1 \sin \xi_1,\ k_{z1} = k_1 \cos \xi_1, \tag{3.32}$$

is used to transform the integration path C from complex k_ρ-plane to the angular spectrum ξ_1-plane and use the substitution

$$\rho = r_2 \sin\theta_2\ ,\ \ z_f + z_s = r_2 \cos\theta_2, \tag{3.33}$$

the Sommerfeld integrals in (4.10) - (4.14) and (4.23) - (4.27) can be expressed as

$$P_\alpha = \frac{1}{\sqrt{2\pi j \Omega_2}} \int_C g_\alpha(\xi_1) e^{-j\Omega_2 \cos(\xi_1 - \theta_2)} d\xi_1 \tag{3.34}$$

where α is the subscript number of the Sommerfeld integrals, the integrands can be expressed as

$$g_1(\xi_1) = [1 - \Gamma_{||}(\xi_1)] \cos\xi_1 \sin\xi_1 \sqrt{\frac{\sin\xi_1}{\sin\theta_2}} H_1(\Omega_2 \sin\theta_2 \sin\xi_1), \tag{3.35}$$

$$g_2(\xi_1) = \left[1 - \Gamma_{||}(\xi_1)\right] \cos^2\xi_1 \sqrt{\frac{\sin\xi_1}{\sin\theta_2}} H_0(\Omega_2 \sin\theta_2 \sin\xi_1), \tag{3.36}$$

$$g_3(\xi_1) = \frac{[1 - \Gamma_{||}(\xi_1)] \cos^2\xi_1}{\sqrt{\sin\theta_2 \sin\xi_1}} H_1(\Omega_2 \sin\theta_2 \sin\xi_1), \tag{3.37}$$

$$g_4(\xi_1) = \frac{[1 + \Gamma_{\perp}(\xi_1)]}{\sqrt{\sin\theta_2 \sin\xi_1}} H_1(\Omega_2 \sin\theta_2 \sin\xi_1), \tag{3.38}$$

$$g_5(\xi_1) = [1 + \Gamma_{\perp}(\xi_1)] \sqrt{\frac{\sin\xi_1}{\sin\theta_2}} H_0(\Omega_2 \sin\theta_2 \sin\xi_1), \tag{3.39}$$

$$g_6(\xi_1) = [1 + \Gamma_{\perp}(\xi_1)] \sin\xi_1 \sqrt{\frac{\sin\xi_1}{\sin\theta_2}} H_1(\Omega_2 \sin\theta_2 \sin\xi_1), \tag{3.40}$$

$$g_7(\xi_1) = [1 + \Gamma_{\perp}(\xi_1)] \cos\xi_1 \sqrt{\frac{\sin\xi_1}{\sin\theta_2}} H_0(\Omega_2 \sin\theta_2 \sin\xi_1), \tag{3.41}$$

$$g_8(\xi_1) = \frac{[1 - \Gamma_{||}(\xi_1)] \cos\xi_1}{\sqrt{\sin\theta_2 \sin\xi_1}} H_1(\Omega_2 \sin\theta_2 \sin\xi_1), \tag{3.42}$$

$$g_9(\xi_1) = \frac{[1 + \Gamma_{\perp}(\xi_1)] \cos\xi_1}{\sqrt{\sin\theta_2 \sin\xi_1}} H_1(\Omega_2 \sin\theta_2 \sin\xi_1), \tag{3.43}$$

$$g_{10}(\xi_1) = \left[1 - \Gamma_{||}(\xi_1)\right]\cos\xi_1 \sqrt{\frac{\sin\xi_1}{\sin\theta_2}} H_0(\Omega_2 \sin\theta_2 \sin\xi_1), \tag{3.44}$$

with

$$\Gamma_{||}(\xi_1) = \frac{\cos\xi_1 - \frac{\delta(\xi_1)}{\epsilon_r}}{\cos\xi_1 + \frac{\delta(\xi_1)}{\epsilon_r}}, \tag{3.45}$$

$$\Gamma_{\perp}(\xi_1) = \frac{\cos\xi_1 - \delta(\xi_1)}{\cos\xi_1 + \delta(\xi_1)}, \tag{3.46}$$

$$\delta(\xi_1) = \sqrt{\epsilon_r - \sin^2\xi_1}. \tag{3.47}$$

and the normalized Hankel function [16] is introduced

$$H_0(z) = j^{-n}\sqrt{\frac{\pi z}{2j}} H_n{}^{(2)}(z) e^{jz} \sim 1 - j\frac{(4n^2 - 1)}{8z} + O(z^{-2}). \tag{3.48}$$

The mapping of pole in k_ρ-plane (3.31) to ξ_1-plane is located at ξ_{1p}, which satisfies

$$\sin\xi_{1p} = \sqrt{\frac{\epsilon_r}{\epsilon_r + 1}}, \qquad \cos\xi_{1p} = -\sqrt{\frac{1}{\epsilon_r + 1}}. \tag{3.49}$$

3.3 Asymptotic Field Expansions for far field

3.3.1 First Order Approximation

By applying (A15), we have

$$E_z^S \sim -\left(1-\Gamma_{||}\right)\cos\theta_2\sin\theta_2 H_1(\Omega_2\sin^2\theta_2)\frac{e^{-j\Omega_2}}{\Omega_2} + Q_p\cos\xi_{1p}\sin\xi_{1p}H_1(\Omega_2\sin\theta_2\sin\xi_{1p})\mathcal{F}(p)\frac{e^{-j\Omega_2}}{\Omega_2}, \tag{3.50}$$

$$E_\rho^S \sim \left(1-\Gamma_{||}\right)\cos^2\theta_2 H_0(\Omega_2\sin^2\theta_2)\frac{e^{-j\Omega_2}}{\Omega_2} - Q_p\cos^2\xi_{1p}H_0(\Omega_2\sin\theta_2\sin\xi_{1p})\mathcal{F}(p)\frac{e^{-j\Omega_2}}{\Omega_2}, \tag{3.51}$$

$$E_\phi^S \sim (1+\Gamma_\perp)H_0(\Omega_2\sin^2\theta_2)\frac{e^{-j\Omega_2}}{\Omega_2}, \tag{3.52}$$

$$H_z^S \sim (1+\Gamma_\perp)\sin\theta_2 H_1(\Omega_2\sin^2\theta_2)\frac{e^{-j\Omega_2}}{\Omega_2}, \tag{3.53}$$

$$H_\rho^S \sim -(1+\Gamma_\perp)\cos\theta_2 H_0(\Omega_2\sin^2\theta_2)\frac{e^{-j\Omega_2}}{\Omega_2}, \tag{3.54}$$

$$H_\phi^S \sim -\left(1-\Gamma_{||}\right)\cos\theta_2 H_0(\Omega_2\sin^2\theta_2)\frac{e^{-j\Omega_2}}{\Omega_2} + Q_p\cos\xi_{1p}H_0(\Omega_2\sin\theta_2\sin\xi_{1p})\mathcal{F}(p)\frac{e^{-j\Omega_2}}{\Omega_2}, \tag{3.55}$$

Where

$$Q_p = -\frac{2{\epsilon_r}^2}{{\epsilon_r}^2-1}\frac{\cos\xi_{1p}}{\sqrt{2j}s_p}\sqrt{\frac{\sin\xi_{1p}}{\sin\theta_2}}. \tag{3.56}$$

3.3.2 Second Order Correction

By using (A16.1), we have the second-order correction for substrative variant modified saddle point method for each field components.

$$\begin{aligned}\triangle \mathrm{E}_z^S \sim & -j\frac{3}{8}\cot\theta_2\left(1-\Gamma_{||}\right)\frac{e^{-j\Omega_2}}{\Omega_2^2}+j\sin\theta_2\left(1-\Gamma_{||}\right)\\ & \left\{\begin{matrix}3\cos\theta_2+\epsilon_r(\epsilon_r-1)\frac{(1-\Gamma_{||})}{2\delta^3}[1-3\cos^2\theta_2(1+\frac{\sin^2\theta_2}{2\delta^2})\\ -\epsilon_r(\epsilon_r-1)\frac{(1-\Gamma_{||})}{2\delta^3}\cos\theta_2\sin^2\theta_2]\end{matrix}\right\}\frac{e^{-j\Omega_2}}{{\Omega_2}^2}\\ & +Q_p\cos\xi_{1p}\sin\xi_{1p}\frac{H_1(\Omega_2\sin\theta_2\sin\xi_{1p})}{2p}\frac{e^{-j\Omega_2}}{\Omega_2},\end{aligned} \tag{3.57}$$

$$\begin{aligned}\triangle \mathrm{E}_\rho^S \sim & -\frac{j}{8}\cot^2\theta_2(1-\Gamma_{||})\frac{e^{-j\Omega_2}}{\Omega_2^2}\\ & +j\left\{\begin{matrix}(1-\Gamma_{||})(1-\cot^2\theta_2-3\cos^2\theta_2)+(1+\Gamma_\perp)(1+\cot^2\theta_2)\\ -\epsilon_r(\epsilon_r-1)\frac{(1-\Gamma_{||})}{2\delta^3}\cos\theta_2[2-3\cos^2\theta_2(1+\frac{\sin^2\theta_2}{2\delta^2})\\ -\epsilon_r(\epsilon_r-1)\frac{(1-\Gamma_{||})}{2\delta^3}\cos\theta_2\sin^2\theta_2]\end{matrix}\right\}\frac{e^{-j\Omega_2}}{{\Omega_2}^2}\\ & -Q_p\cos^2\xi_{1p}[\frac{-j\mathcal{F}(p)}{\Omega_2\sin\theta_2\sin\xi_{1p}}+\frac{H_0(\Omega_2\sin\theta_2\sin\xi_{1p})}{2p}]\frac{e^{-j\Omega_2}}{\Omega_2},\end{aligned} \tag{3.58}$$

$$\begin{aligned}\triangle \mathrm{E}_\phi^S \sim & -\frac{j}{8\sin^2\theta_2}(1+\Gamma_\perp)\frac{e^{-j\Omega_2}}{\Omega_2^2}\\ & -j\left\{\begin{matrix}(1+\Gamma_\perp)(1+\cot^2\theta_2)-(1-\Gamma_{||})\cot^2\theta_2\\ -\frac{\Gamma_\perp}{\delta}[\cos\theta_2(1+\frac{\epsilon_r}{\delta^2})+\frac{2}{\delta}\sin^2\theta_2]\end{matrix}\right\}\frac{e^{-j\Omega_2}}{{\Omega_2}^2}\\ & -Q_p\frac{j\cos^2\xi_{1p}}{\sin\theta_2\sin\xi_{1p}}\mathcal{F}(p)\frac{e^{-j\Omega_2}}{\Omega_2^2},\end{aligned} \tag{3.59}$$

$$\begin{aligned}\triangle \mathrm{H}_z^S \sim & \ j\frac{3}{8\sin^2\theta_2}(1+\Gamma_\perp)\frac{e^{-j\Omega_2}}{\Omega_2^2}\\ & -j\sin\theta_2\{(1+\Gamma_\perp)-\frac{\Gamma_\perp}{\delta}[\cos\theta_2(3+\frac{\epsilon_r}{\delta^2})+\frac{2}{\delta}\sin^2\theta_2]\}\frac{e^{-j\Omega_2}}{\Omega_2^2}\end{aligned} \tag{3.60}$$

$$\triangle \mathrm{H}_{\rho}^{S} \sim j\frac{\cos\theta_2}{8\sin^2\theta_2}(1+\Gamma_{\perp})\frac{e^{-j\Omega_2}}{\Omega_2^2}$$
$$+j\left\{\begin{array}{c}\cos\theta_2[(1+\Gamma_{\perp})(2+\cot^2\theta_2)-(1-\Gamma\ )(1+\cot^2\theta_2)]\\ +\frac{\Gamma_{\perp}}{\delta}[2-\cos^2\theta_2(3+\frac{\epsilon_r}{\delta^2})-\frac{2}{\delta}\cos\theta_2\sin^2\theta_2]\end{array}\right\}\frac{e^{-j\Omega_2}}{{\Omega_2}^2} \tag{3.61}$$
$$+Q_p\frac{j\cos\xi_{1p}}{\sin\theta_2\sin\xi_{1p}}\mathcal{F}(p)\frac{e^{-j\Omega_2}}{\Omega_2^2},$$

$$\triangle \mathrm{E}_{\rho}^{S} \sim j\frac{\cos\theta_2}{8\sin^2\theta_2}(1-\Gamma_{||})\frac{e^{-j\Omega_2}}{\Omega_2^2}$$
$$+j\left\{\begin{array}{c}\cos\theta_2[-(1+\Gamma_{\perp})(1+\cot^2\theta_2)+(1-\Gamma_{||})(2+\cot^2\theta_2)]\\ +\epsilon_r(\epsilon_r-1)\frac{(1-\Gamma_{||})^2}{4\delta^3}[2-\cos^2\theta_2(4+\frac{3}{\delta^2}\sin^2\theta_2)\\ -\epsilon_r(\epsilon_r-1)\frac{(1-\Gamma_{||})}{\delta^3}\cos\theta_2\sin^2\theta_2]\end{array}\right\}\frac{e^{-j\Omega_2}}{{\Omega_2}^2} \tag{3.62}$$
$$+\ Q_p\cos\xi_{1p}[\frac{-j\mathcal{F}(p)}{\Omega_2\sin\theta_2\sin\xi_{1p}}+\frac{H_0(\Omega_2\sin\theta_2\sin\xi_{1p})}{2p}]\frac{e^{-j\Omega_2}}{\Omega_2},$$

3.3.3 Complete Second-Order Field Expansions

By combine the first-order approximation in 3.3.1 with the second-order correction terms in 3.3.2, we obtain

$$
\begin{aligned}
E_z \sim & -\cos\phi \frac{j\eta_1 {k_1}^2}{4\pi}\langle -\sin\theta_1\cos\theta_1[1-3(\frac{j}{\Omega_1}+\frac{1}{\Omega_1^2})]\frac{e^{-\mathrm{j}\Omega_1}}{\Omega_1} \\
& +\sin\theta_2\cos\theta_2[\Gamma_{||}-3(\frac{j}{\Omega_2}+\frac{1}{\Omega_2^2})]\frac{e^{-\mathrm{j}\Omega_2}}{\Omega_2}+j\sin\theta_2(1-\Gamma_{||}) \\
& \left\{\begin{matrix} 3\cos\theta_2+\epsilon_r(\epsilon_r-1)\frac{(1-\Gamma_{||})}{2\delta^3}[1-3\cos^2\theta_2(1+\frac{\sin^2\theta_2}{2\delta^2}) \\ -\epsilon_r(\epsilon_r-1)\frac{(1-\Gamma_{||})}{2\delta^3}\cos\theta_2\sin^2\theta_2] \end{matrix}\right\}\frac{e^{-j\Omega_2}}{{\Omega_2}^2} \\
& +Q_p\cos\xi_{1p}\sin\xi_{1p}H_1(\Omega_2\sin\theta_2\sin\xi_{1p})[\mathcal{F}(p)+\frac{1}{2p}]\frac{e^{-j\Omega_2}}{\Omega_2}\rangle,
\end{aligned}
\tag{3.63}
$$

$$
\begin{aligned}
E_\rho \sim & -\cos\phi \frac{j\eta_1 {k_1}^2}{4\pi}\langle[\cos^2\theta_1+(2-3\cos^2\theta_1)(\frac{j}{\Omega_1}+\frac{1}{\Omega_1^2})]\frac{e^{-j\Omega_1}}{\Omega_1} \\
& -[\Gamma_{||}\cos^2\theta_2+(2-3\cos^2\theta_2)(\frac{j}{\Omega_2}+\frac{1}{\Omega_2^2})]\frac{e^{-j\Omega_2}}{\Omega_2} \\
& +j\left\{\begin{matrix} (1-\Gamma_{||})(1-\cot^2\theta_2-3\cos^2\theta_2)+(1+\Gamma_\perp)(1+\cot^2\theta_2) \\ -\epsilon_r(\epsilon_r-1)\frac{(1-\Gamma_{||})}{2\delta^3}\cos\theta_2[2-3\cos^2\theta_2(1+\frac{\sin^2\theta_2}{2\delta^2}) \\ -\epsilon_r(\epsilon_r-1)\frac{(1-\Gamma_{||})}{2\delta^3}\cos\theta_2\sin^2\theta_2] \end{matrix}\right\}\frac{e^{-j\Omega_2}}{{\Omega_2}^2} \\
& -Q_p\cos^2\xi_{1p}[\frac{(H_0(\Omega_2\sin\theta_2\sin\xi_{1p})-j)\mathcal{F}(p)}{\Omega_2\sin\theta_2\sin\xi_{1p}}+\frac{H_0(\Omega_2\sin\theta_2\sin\xi_{1p})}{2p}]\frac{e^{-j\Omega_2}}{\Omega_2}\rangle,
\end{aligned}
\tag{3.64}
$$

$$
\begin{aligned}
E_\phi = & \sin\phi \frac{j\eta_1 {k_1}^2}{4\pi}\langle[1-(\frac{j}{\Omega_1}+\frac{1}{\Omega_1^2})]\frac{e^{-\mathrm{j}\Omega_1}}{\Omega_1}+[\Gamma_\perp+(\frac{j}{\Omega_2}+\frac{1}{\Omega_2^2})]\frac{e^{-\mathrm{j}\Omega_2}}{\Omega_2} \\
& -j\left\{\begin{matrix} (1+\Gamma_\perp)(1+\cot^2\theta_2)-(1-\Gamma_{||})\cot^2\theta_2 \\ -\frac{\Gamma_\perp}{\delta}[\cos\theta_2(1+\frac{\epsilon_r}{\delta^2})+\frac{2}{\delta}\sin^2\theta_2] \end{matrix}\right\}\frac{e^{-j\Omega_2}}{{\Omega_2}^2} \\
& -Q_p\frac{j\cos^2\xi_{1p}}{\sin\theta_2\sin\xi_{1p}}\mathcal{F}(p)\frac{e^{-j\Omega_2}}{\Omega_2^2}\rangle,
\end{aligned}
\tag{3.65}
$$

$$H_z = \sin\phi \frac{j{k_1}^2}{4\pi} \langle \sin\theta_1 (1 - \frac{j}{\Omega_1}) \frac{e^{-\mathrm{j}\Omega_1}}{\Omega_1} + \sin\theta_2 (\Gamma_\perp + \frac{j}{\Omega_2}) \frac{e^{-\mathrm{j}\Omega_2}}{\Omega_2}$$
$$-j\sin\theta_2 \{(1 + \Gamma_\perp) - \frac{\Gamma_\perp}{\delta} [\cos\theta_2 (3 + \frac{\epsilon_r}{\delta^2}) + \frac{2}{\delta} \sin^2\theta_2]\} \frac{e^{-j\Omega_2}}{\Omega_2^2} \tag{3.66}$$

$$H_\rho = \sin\phi \frac{j{k_1}^2}{4\pi} \langle -\cos\theta_1 (1 - \frac{j}{\Omega_1}) \frac{e^{-\mathrm{j}\Omega_1}}{\Omega_1} - \cos\theta_2 (\Gamma_\perp + \frac{j}{\Omega_2}) \frac{e^{-\mathrm{j}\Omega_2}}{\Omega_2}$$
$$+j \left\{ \begin{matrix} \cos\theta_2 [(1 + \Gamma_\perp)(2 + \cot^2\theta_2) - (1 - \Gamma_{||})(1 + \cot^2\theta_2)] \\ + \frac{\Gamma_\perp}{\delta} [2 - \cos^2\theta_2 (3 + \frac{\epsilon_r}{\delta^2}) - \frac{2}{\delta} \cos\theta_2 \sin^2\theta_2] \end{matrix} \right\} \frac{e^{-j\Omega_2}}{{\Omega_2}^2} \tag{3.67}$$
$$+Q_p \frac{j\cos\xi_{1p}}{\sin\theta_2 \sin\xi_{1p}} \mathcal{F}(p) \frac{e^{-j\Omega_2}}{\Omega_2^2} \rangle,$$

$$H_\phi = \cos\phi \frac{j{k_1}^2}{4\pi} \langle -\cos\theta_1 (1 - \frac{j}{\Omega_1}) \frac{e^{-\mathrm{j}\Omega_1}}{\Omega_1} + \cos\theta_2 (\Gamma_{||} - \frac{j}{\Omega_2}) \frac{e^{-\mathrm{j}\Omega_2}}{\Omega_2}$$
$$+j \left\{ \begin{matrix} \cos\theta_2 \left[-(1 + \Gamma_\perp)(1 + \cot^2\theta_2) + \left(1 - \Gamma_{||}\right)(2 + \cot^2\theta_2) \right] \\ + \epsilon_r (\epsilon_r - 1) \frac{\left(1 - \Gamma_{||}\right)^2}{4\delta^3} [2 - \cos^2\theta_2 (4 + \frac{3}{\delta^2} \sin^2\theta_2) \\ - \epsilon_r (\epsilon_r - 1) \frac{\left(1 - \Gamma_{||}\right)}{\delta^3} \cos\theta_2 \sin^2\theta_2] \end{matrix} \right\} \frac{e^{-j\Omega_2}}{{\Omega_2}^2} \tag{3.68}$$
$$+Q_p \cos\xi_{1p} [(H_0(\Omega_2 \sin\theta_2 \sin\xi_{1p}) - \frac{j}{\Omega_2 \sin\theta_2 \sin\xi_{1p}}) \mathcal{F}(p)$$
$$+ \frac{H_0(\Omega_2 \sin\theta_2 \sin\xi_{1p})}{2p}] \frac{e^{-j\Omega_2}}{\Omega_2} \rangle,$$

3.3.4 Surface-to-Surface Propagation Formulas

For the surface-to-surface propagation case, where $z_f = z_s = 0$, the formula (3.63) - (3.68) reduce to

$$E_z \sim \cos\phi \frac{\eta_1 {k_1}^2}{2\pi} \{ \frac{\epsilon_r}{\sqrt{\epsilon_r - 1}} \frac{e^{-jk_0\rho}}{(k_0\rho)^2} - j\frac{Q_p}{2} \cos\xi_{1p} \sin\xi_{1p} H_1(k_p\rho)[\mathcal{F}(p) + \frac{1}{2p}] \frac{e^{-jk_0\rho}}{k_0\rho} \}, \tag{3.69}$$

$$E_\rho \sim \cos\phi \frac{\eta_1 {k_1}^2}{4\pi} \langle \frac{e^{-jk_0\rho}}{(k_0\rho)^2} + j\frac{Q_p}{2} \cos^2\xi_{1p} \{ H_0(k_p\rho)[\mathcal{F}(p) + \frac{1}{2p}] + \frac{\mathcal{F}(p)}{jk_p\rho} \} \frac{e^{-jk_0\rho}}{k_0\rho} \rangle, \tag{3.70}$$

$$E_\phi \sim \sin\phi \frac{\eta_1 {k_1}^2}{2\pi} \langle \frac{1}{\epsilon_r - 1} + \frac{Q_p}{2} \cot\xi_{1p} \cos\xi_{1p} \mathcal{F}(p) \rangle \frac{e^{-jk_0\rho}}{(k_0\rho)^2}, \tag{3.71}$$

$$H_z \sim \sin\phi \frac{{k_1}^2}{2\pi} (\frac{1}{\epsilon_r - 1}) \frac{e^{-jk_0\rho}}{(k_0\rho)^2}, \tag{3.72}$$

$$H_\rho \sim \sin\phi \frac{{k_1}^2}{2\pi} [\frac{1}{\sqrt{\epsilon_r - 1}} - \frac{Q_p}{2} \cot\xi_{1p} \mathcal{F}(p)] \frac{e^{-jk_0\rho}}{(k_0\rho)^2}, \tag{3.73}$$

$$H_\phi \sim -\cos\phi \frac{{k_1}^2}{2\pi} \langle \frac{\epsilon_r}{\sqrt{\epsilon_r - 1}} \frac{e^{-jk_0\rho}}{(k_0\rho)^2} - j\frac{Q_p}{2} \cos\xi_{1p} \{ H_0(k_p\rho)[\mathcal{F}(p) + \frac{1}{2p}] + \frac{\mathcal{F}(p)}{\mathrm{j}k_p\rho} \} \frac{e^{-jk_0\rho}}{k_0\rho} \rangle. \tag{3.74}$$

3.4 Numerical Results

Table 3.1: Model considered for ordinary(left) and plasmonic(right) medium.

	Seawater @ f = 20 MHz	Gold @ λ_0=633nm
ε_r'	80	-
σ	3.5 S/m	-
ε_r	$80 - j\,3.14564 \times 10^3$	$-11.53015 - j\,1.20367$
k_p/k_0	$0.999996 - j\,1.5885 \times 10^{-4}$	$1.045833 - j\,5.1228 \times 10^{-3}$
z_s	10 m	200 nm

Two high-contrast problems listed in Table 3.1 are evaluated numerically by the asymptotic formulas compared with the exact Sommerfeld integral results. The ordinary medium [22] and the plasmonic medium is represented by the sea water and gold in the two-layer model. To evaluate the field components near the interface, the modified saddle point method should be applied because the pole singularity - on the left of k_0 for seawater and on the right of k_0 for gold - is close to the saddle point. The first- and second-order MSP approximations are computed in the following tables and plots. MSP1 and MSP2 stands for the first- and second-order subtractive variants of the MSP method. The results from Norton-Bannister formulation and King formulation are denoted as N-B and King.

In Figure 3.2 and 3.3, the normalized field patterns from $\theta_2 = 1$ (near the z axis) to $\theta_2 = 90$ (on the interface) in far-field for the seawater and gold problems are computed by rigorous numerical integration of Sommerfeld integrals (solid line) and by MSP2 (dashed line), and the exact and MSP2 results are visually indistinguishable. Note that the $\sin\phi$ and $\cos\phi$ are set to 1. In Figure 3.3, a strong surface wave is observed in some field components which is contributed from SPP.

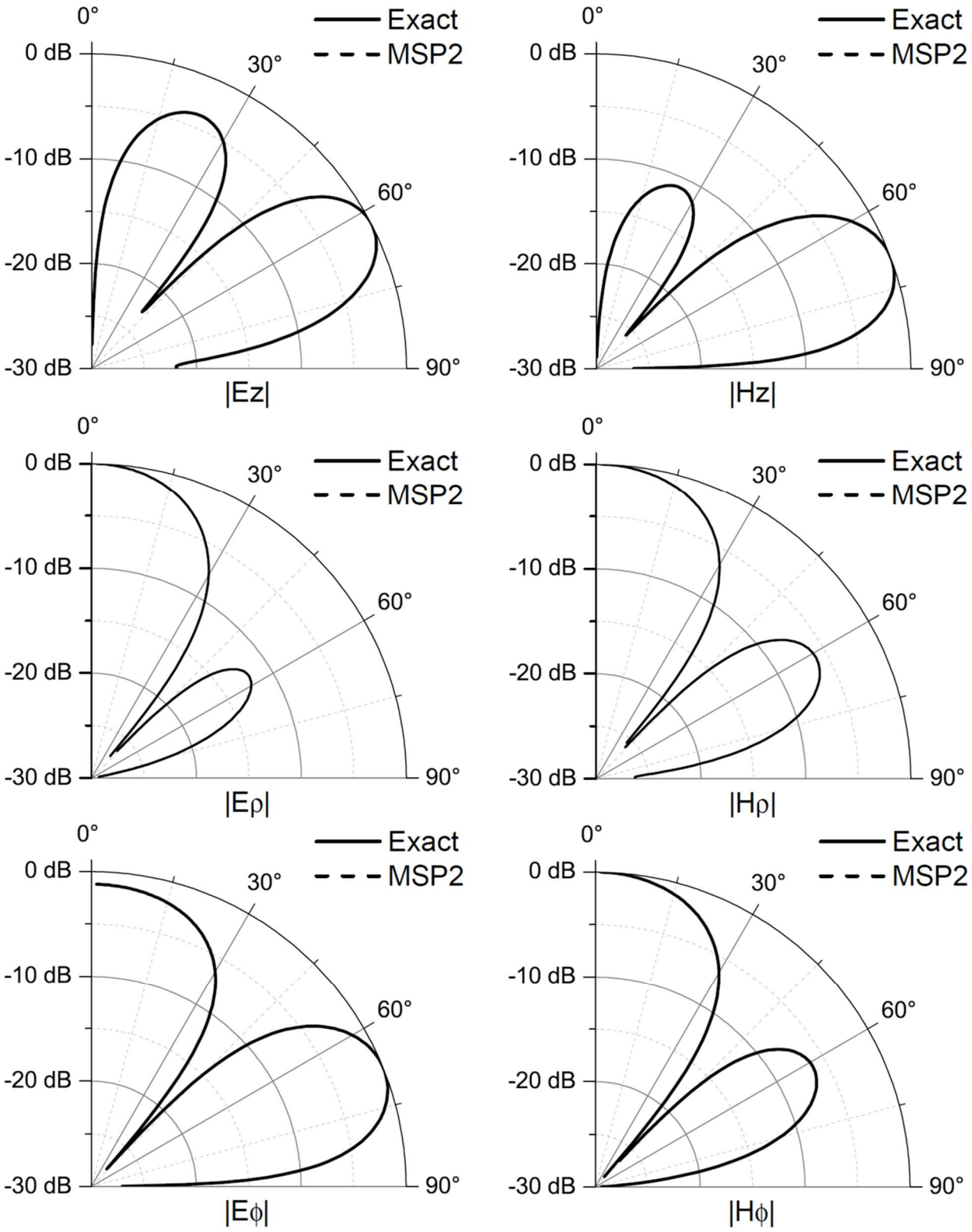

Figure 3.2: Field patterns for seawater case at k_0r=100.

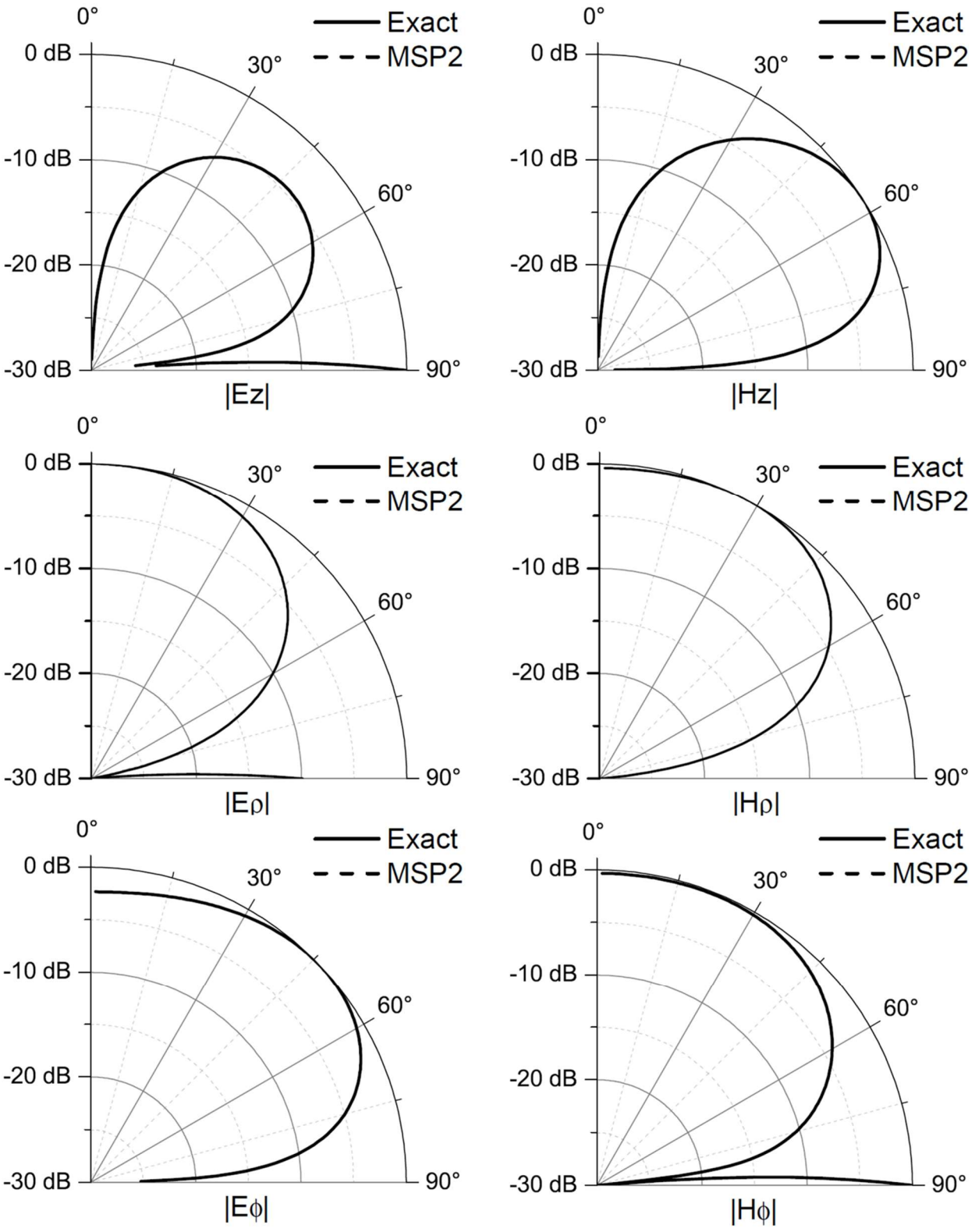

Figure 3.3: Field patterns for gold case at k_0r=100.

In in Table 3.2 and 3.3, the relative root-mean-square (RMS) errors for plotting field patterns, only computed in the range $k_0 r_2 \sin^2 \theta_2 > 10$, are listed for different field components. As expected, MSP2 is more accurate than MSP1 in gold and seawater problems. Except E_z in the seawater case, the MSP2 results are more accurate than N-B and King, especially in the plasmonic case (gold problem).

Table 3.2: RMS Errors (%) in field patterns at $k_0 r = 100$ for the seawater problem.

	MSP1	MSP2	N-B	King
E_z	1.9×10^{-1}	2.6×10^{-2}	4.0×10^{-3}	6.1×10^{-3}
E_ρ	4.1×10^{-1}	6.1×10^{-3}	8.4×10^{-3}	7.6×10^{-3}
E_ϕ	1.5×10^{-1}	6.6×10^{-4}	2.0×10^{-3}	2.0×10^{-3}
H_z	2.9×10^{-1}	3.4×10^{-3}	1.3×10^{-3}	1.7×10^{-3}
H_ρ	2.6×10^{-1}	2.6×10^{-3}	1.4×10^{-1}	1.4×10^{-1}
H_ϕ	2.2×10^{-1}	7.7×10^{-3}	2.0×10^{-2}	1.7×10^{-2}

Table 3.3: RMS Errors (%) in field patterns at $k_0 r = 1000$ for the seawater problem.

	MSP1	MSP2	N-B	King
E_z	1.5	6.2×10^{-2}	7.0	7.3
E_ρ	8.9×10^{-1}	1.8×10^{-2}	4.0	4.0
E_ϕ	2.9	2.0×10^{-2}	1.4	1.4
H_z	1.2	3.2×10^{-2}	5.3×10^{-1}	1.4
H_ρ	5.8	6.9×10^{-2}	4.4	4.4
H_ϕ	7.3×10^{-1}	2.6×10^{-2}	5.6	5.9

In Figure 3.4 and 3.5, the magnitude of the fields along z = h surface computed by MSP2 are plotted for the two problems, which are normalized to the maximum field magnitude. In the seawater case, the dB scale plot covers the four-decade range from $10 < k_0\rho < 10^4$. Three-decade range are covered from $10^2 < k_0\rho < 10^6$ in the gold case. In the seawater case, Figure 3.4, E_ϕ dominates E_ρ, which can also be observed in the field pattern plots in Figure 3.2. The dip in the near-intermediate range for E_z, E_ρ and H_ϕ is caused by the cancellation between the direct and image waves. In the gold case, Figure 3.5, the strong SPP influence is observed in E_z, E_ρ and H_ϕ fields decay $O(\rho^{-1/2})$ in the intermate range and becomes $O(\rho^{-2})$. The wiggles between the $O(\rho^{-1/2})$ and $O(\rho^{-2})$ transition region come from the interference between the lateral wave and pole wave with the comparable magnitude. Also note that all the fields finally decay as $O(\rho^{-2})$ when $k_0\rho$ is large .

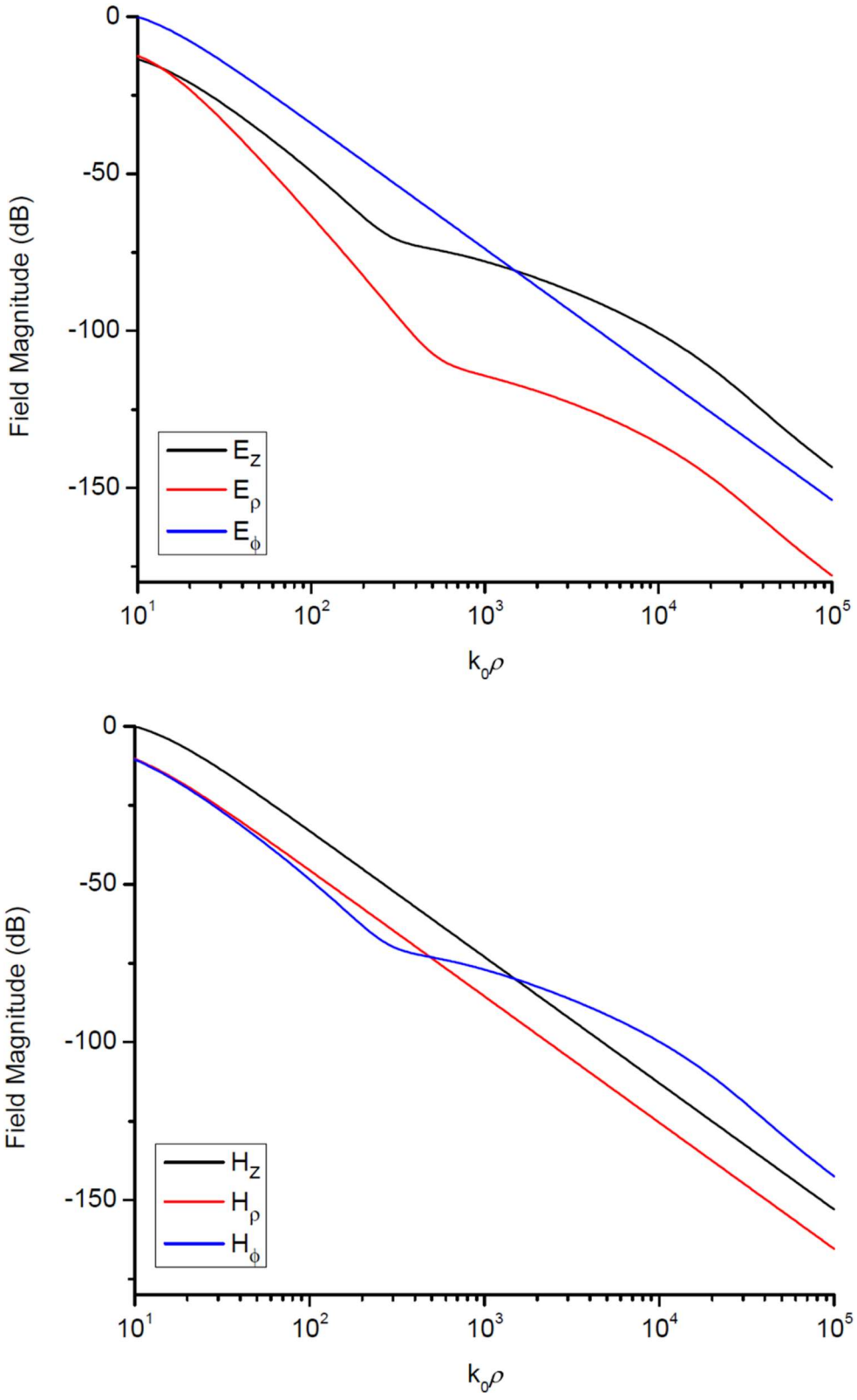

Figure 3.4: Field along the z=h surface for the seawater case computed by MSP2.

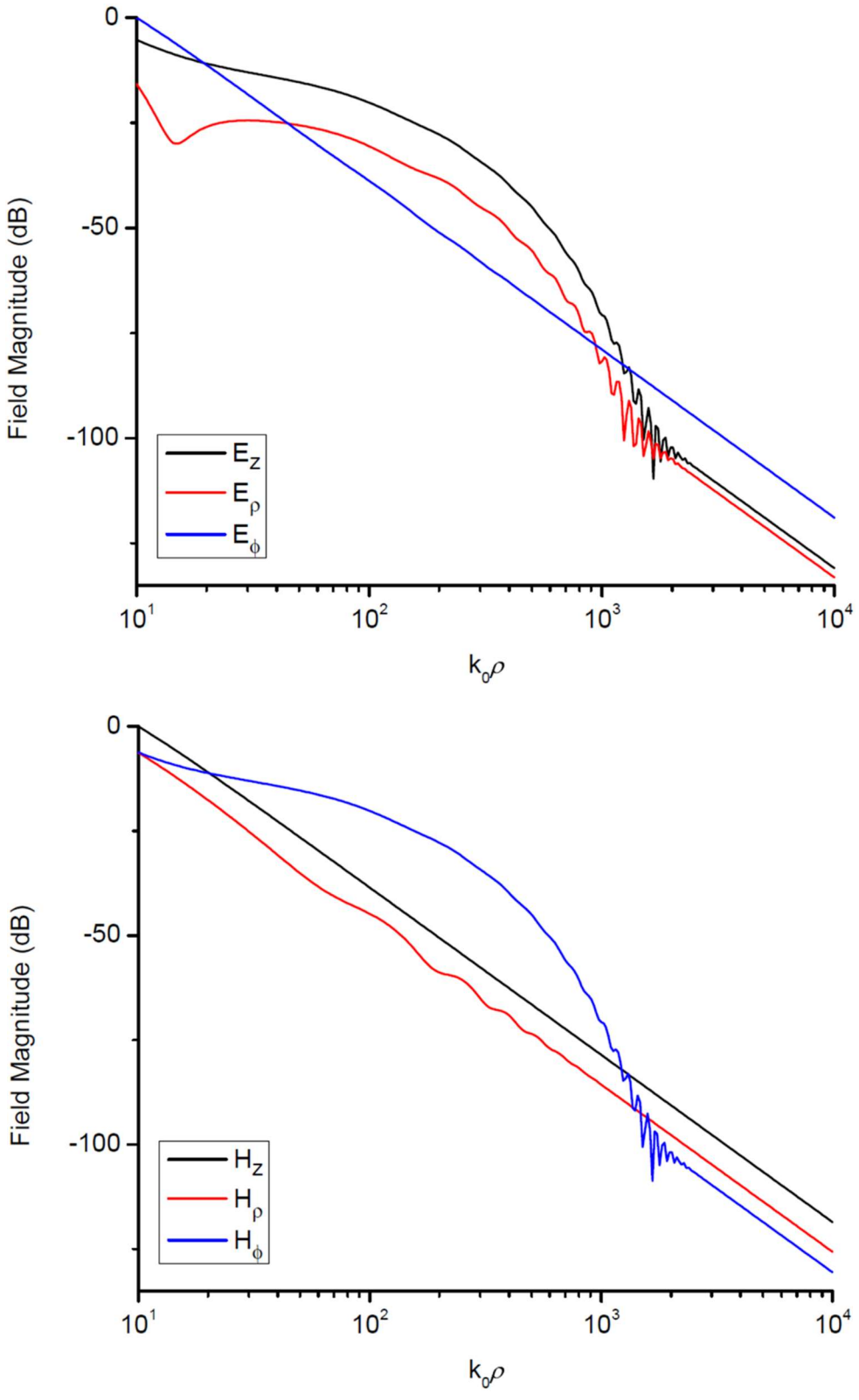

Figure 3.5: Field along the z=h surface for the gold case computed by MSP2.

The surface fields RMS percent errors computed in Figure 3.4 and 3.5 are listed in Tables 3.6 and 3.7. MSP2 performs better than the other methods, except E_z and H_ρ fields in the seawater case. To understand the large amounts of errors from N-B and King (especially) near-surface field results in the plasmonic case, the fields computed by MSP2 and King are plotted by comparing with the exact Sommerfeld integral results in Figure 3.6. We can notice that King results are slightly shifted to the exact.

Table 3.4: RMS Errors (%) in surface field at z = h for the sea water problem.

	MSP1	MSP2	N-B	King
E_z	3.3×10^{-1}	8.8×10^{-2}	4.1×10^{-2}	3.4×10^{-2}
E_ρ	1.0×10^{-1}	1.7×10^{-2}	6.5×10^{-2}	6.0×10^{-2}
E_ϕ	4.3×10^{-3}	9.2×10^{-6}	1.4×10^{-4}	1.4×10^{-4}
H_z	7.5×10^{-3}	5.6×10^{-5}	1.3×10^{-4}	1.4×10^{-4}
H_ρ	6.2×10^{-1}	2.2×10^{-3}	6.3×10^{-4}	5.3×10^{-4}
H_ϕ	3.2×10^{-1}	2.9×10^{-2}	8.4×10^{-2}	8.3×10^{-2}

Table 3.5: RMS Errors (%) in surface field at z = h for the gold problem.

	MSP1	MSP2	N-B	King
E_z	1.1×10	2.7×10^{-2}	4.6×10	1.6×10^{2}
E_ρ	1.5	7.1×10^{-3}	3.9×10	1.5×10^{2}
E_ϕ	2.0	9.5×10^{-3}	1.1	1.3
H_z	1.6	1.5×10^{-2}	8.8×10^{-1}	1.0
H_ρ	1.5×10	7.5×10^{-2}	1.3	5.8
H_ϕ	2.8	1.3×10^{-2}	4.6×10	1.6×10^{2}

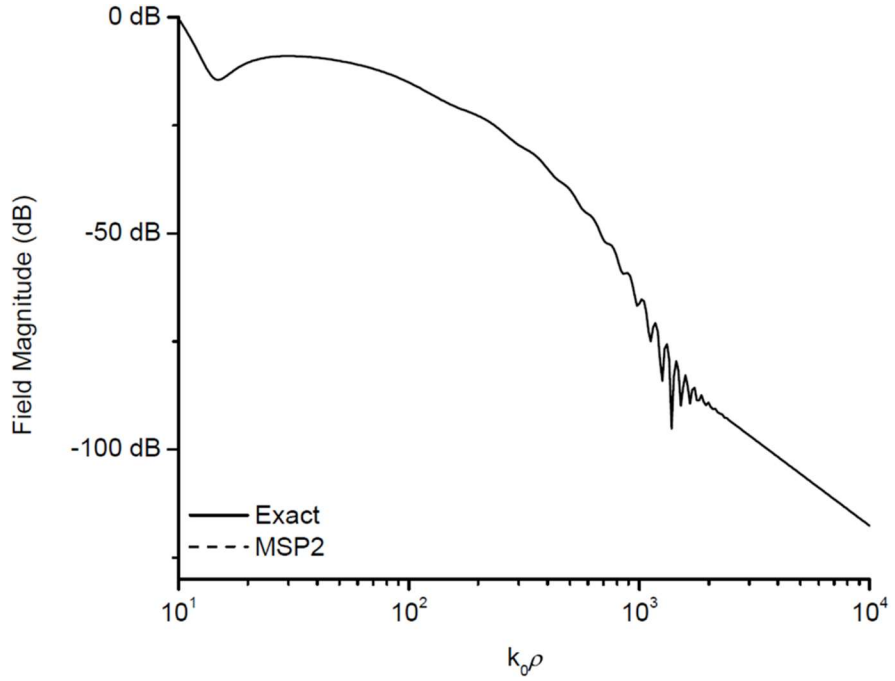

(a)

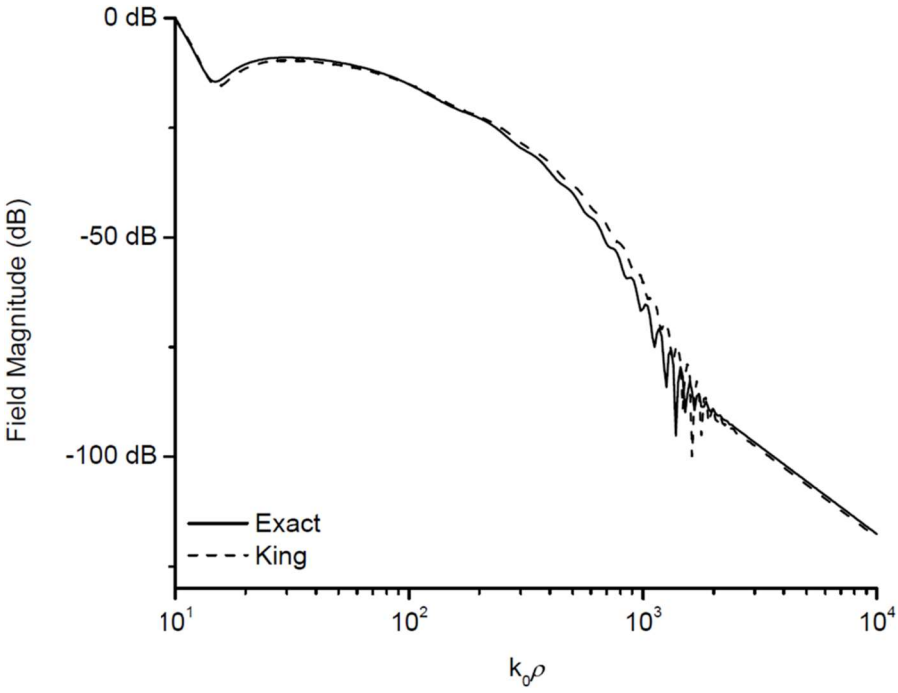

(b)

Figure 3.6: $|E_z|$ surface fields for the gold case computed by (a)MSP2 and (b)King, and compared with the exact results.

CHAPTER IV

CONCLUSION AND FUTURE WORKS

4.1 Conclusion

New asymptotic formulas for the electromagnetic fields of vertical and horizontal electric dipoles radiating on or above an imperfectly conducting half-space have been developed using the modified saddle point method. The two variants of the modified saddle point method – subtractive and multiplicative - are also derived and are proved to be equal to each other when the number of terms in the expansion goes to infinity. From RMS errors of the numerical results of the field patterns and surface field plots, the new second-order asymptotic formulation has been found to be more accurate than the Norton-Bannister and King methods, especially in the case of plasmonic media. The contribution from this thesis were published in [23,29,41].

4.2 Future works

With the growing applications of the underwater communication, underground sensors network, and smart farming, the research on the approximation for the Sommerfeld integrals in transmitted wave has come to the stage. While the asymptotic formula for the reflect wave has been developed by different methods for the full top layer space, the asymptotic formula for the transmitted wave for the full angel in bottom layer has not been derived. The saddle point method can be used to derive the refracted wave formulas, which satisfied Snell's law. However, this method is only applicable when the source and field points are away from the interface [10-12] given that the branch point singularity is not taken into consideration in the derivation. When the observation point is near the interface, the second-order approximation of the saddle point method and the BCI are needed to be considered and the transmitted field near the interface is given by

Brekhovskikh [12]. In the recent study by Michalski and Mosig [51], the transmitted field formula is derived by using the MSP method when the source point near the interface. However, the field expression fails when the saddle point is near the branch point [51,52].

One limitation of the transmitted field formula applications is that one of the observation or field points must be close to the interface, and even the field point is on the interface to remove the branch-cut singularity in the exponent of Sommerfeld integral. For example, the transmitted field formula in lossless media is derived using the uniform asymptotic expansion (UAE) method and the field near the critical point can be predicted by this formula [49]. In Dinh [50], the observation point is limited to the surface and the related exponential term is expanded in infinite series to derive their asymptotic formula. In Lihh [30], even with the limitation of the field point being right on the interface, the transmitted field formula is applicable only when the observation angle is around the critical angle. The problem can also be observed in Temme [47], and no singularity in the exponent in the standard form of the integral is used in asymptotic analysis.

In the UAE method, the parabolic cylinder function (PCF) is used to obtain the leading order term [45,46,53]. The PCF makes the UAE method is not only applicable to the observation angle around the critical angle, but also can handle the saddle point coalescing with the branch point when both layers are lossless [45]. However, it is tough to obtain the correct value of PCF, especially where there is a complex value input argument. The most reliable subroutine to compute the parabolic cylinder function proposed by Gil can only work for the real argument [31]. Even though the commercial softer ware has the built-in PCF to obtain the value for the complex argument, it is not reliable [48]. According to my last contact with Dr. Gil via email, it is known that they are considering on expanding their previous work to cover complex arguments and will publish it in the near future.

REFERENCES

[1] A. Sommerfeld, “Über die Ausbreitung der Wellen in der drahtlosen Telegraphie,” *Annalen der Physik,* vol. 333, no. 4, pp. 665-736, 1909.

[2] R. E. Collin, “Hertzian dipole radiating over a lossy earth or sea: Some early and late 20th-century controversies,” *IEEE Antennas and Propagation Magazine,* vol. 46, no. 2, pp. 64-79, 2004.

[3] J. Maclean and G. Wu, *Radiowave propagation over ground*. Springer, 1993.

[4] K. A. Norton, “The propagation of radio waves over the surface of the earth and in the upper atmosphere,” *Proceedings of the Institute of Radio Engineers,* vol. 25, no. 9, pp. 1203-1236, 1937.

[5] P. R. Bannister, “New formulas that extend Norton's farfield elementary dipole equations to the quasi-nearfield range,” NAVAL UNDERWATER SYSTEMS CENTER NEW LONDON CT, 1984.

[6] H. Ott, “Die Sattelpunktsmethode in der Umgebung eines Pols. Mit Anwendungen auf die Wellenoptik und Akustik,” *Annalen der Physik,* vol. 435, no. 6-7, pp. 393-403, 1943.

[7] B. L. van der Waerden, “On the method of saddle points,” *Applied Scientific Research, Section B,* vol. 2, no. 1, pp. 33-45, 1952.

[8] J. Wait and W. Fraser, “Radiation from a vertical dipole over a stratified ground (Part II),” *Transactions of the IRE Professional Group on Antennas and Propagation,* vol. 2, no. 4, pp. 144-146, 1954.

[9] B. Ung and Y. Sheng, “Optical surface waves over metallo-dielectric nanostructures: Sommerfeld integrals revisited,” *Optics express,* vol. 16, no. 12, pp. 9073-9086, 2008.

[10] A. Ishimaru, *Electromagnetic wave propagation, radiation, and scattering.* Prentice Hall, 1991.

[11] L. B. Felsen and N. Marcuvitz, *Radiation and Scattering of Waves.* Prentice Hall, 1973.

[12] L. M. Brekhovskikh, *Waves in Layered Media*, 2nd ed., Academic Press,1980.

[13] A. Biggs and H. Swarm, "Radiation fields from an electric dipole antenna in homogeneous Antarctic terrain," *IEEE Transactions on Antennas and Propagation,* vol. 16, no. 2, pp. 201-208, 1968.

[14] J. R. Wait, "The electromagnetic fields of a horizontal dipole in the presence of a conducting half-space," *Canadian Journal of Physics,* vol. 39, no. 7, pp. 1017-1028, 1961.

[15] G. Tyras, *Radiation and propagation of electromagnetic waves*. Academic Press, 1969.

[16] K. A. Michalski, "Electromagnetic field computation in planar multilayers," *Encyclopedia of RF and microwave engineering,* 2005.

[17] L. Novotny, "Allowed and forbidden light in near-field optics. I. A single dipolar light source," *JOSA A,* vol. 14, no. 1, pp. 91-104, 1997.

[18] P. Lalanne, J.-P. Hugonin, H. Liu, and B. Wang, "A microscopic view of the electromagnetic properties of sub-λ metallic surfaces," *Surface Science Reports,* vol. 64, no. 10, pp. 453-469, 2009.

[19] R. D. Nevels and K. A. Michalski, "On the behavior of surface plasmons at a metallo-dielectric interface," *Journal of Lightwave Technology,* vol. 32, no. 19, pp. 3299-3305, 2014.

[20] K. A. Michalski and R. D. Nevels, "On the groundwave excited by a vertical Hertzian dipole over a planar conductor: Second-order asymptotic expansion with applications to plasmonics," *IEEE Transactions on Microwave Theory and Techniques,* vol. 65, no. 4, pp. 1133-1140, 2017.

[21] J. R. Wait, *Lectures on Wave Propagation Theory*. Pergamon, 1981.

[22] S. F. Mahmoud and Y. M. Antar, "High frequency ground wave propagation," *IEEE Transactions on Antennas and Propagation,* vol. 62, no. 11, pp. 5841-5846, 2014.

[23] K. A. Michalski and H.-I. Lin, "On the far-zone electromagnetic field of a vertical Hertzian dipole over an imperfectly conducting half-space with extensions to plasmonics," *Radio Science,* vol. 52, no. 7, pp. 798-810, 2017.

[24] K. A. Michalski, "Extrapolation methods for Sommerfeld integral tails," *IEEE Transactions on Antennas and Propagation,* vol. 46, no. 10, pp. 1405-1418, 1998.

[25] K. A. Michalski and J. R. Mosig, "Efficient computation of Sommerfeld integral tails–methods and algorithms," *Journal of Electromagnetic Waves and Applications,* vol. 30, no. 3, pp. 281-317, 2016.

[26] M. Abramowitz and I. A. Stegun, *Handbook of mathematical functions with formulas, graphs, and mathematical tables*. US Government printing office, 1964.

[27] K. A. Michalski and J. R. Mosig, "The Sommerfeld halfspace problem redux: Alternative field representations, role of Zenneck and surface plasmon waves," *IEEE Transactions on Antennas and Propagation,* vol. 63, no. 12, pp. 5777-5790, 2015.

[28] M. R. Zaghloul and A. N. Ali, "Algorithm 916: computing the Faddeyeva and Voigt functions," *ACM Transactions on Mathematical Software (TOMS),* vol. 38, no. 2, pp. 1-22, 2012.

[29] K. A. Michalski and H.-I. Lin, "On the Sommerfeld half-space problem: appraisal of approximate solutions with extensions to plasmonics," *Journal of Electromagnetic Waves and Applications,* vol. 32, no. 4, pp. 483-503, 2018.

[30] W.S. Lihh, "Asymptotic fields in frequency and time domains generated by a point source at the horizontal interface between vertically uniaxial media," *IEEE transactions on antennas and propagation,* vol. 55, no. 10, pp. 2733-2745, 2007.

[31] A. Gil, J. Segura, and N. M. Temme, “Algorithm 914: parabolic cylinder function W (a, x) and its derivative,” *ACM Transactions on Mathematical Software (TOMS),* vol. 38, no. 1, pp. 1-5, 2011.

[32] R. W. King, “Electromagnetic field of a vertical dipole over an imperfectly conducting half-space,” *Radio Science,* vol. 25, no. 2, pp. 149-160, 1990.

[33] K. A. Michalski and D. R. Jackson, “Equivalence of the king and norton–bannister theories of dipole radiation over ground with extensions to plasmonics,” *IEEE Transactions on Antennas and Propagation,* vol. 64, no. 12, pp. 5251-5261, 2016.

[34] G. Bernard and A. Ishimaru, “On complex waves,” in *Proceedings of the Institution of Electrical Engineers*, 1967, vol. 114, no. 1: IET, pp. 43-49.

[35] B. Kockel, “Die Sommerfeldsche Bodenwelle,” *Annalen der Physik,* vol. 456, no. 1-3, pp. 145-156, 1957.

[36] A. Y. Nikitin, S. G. Rodrigo, F. García-Vidal, and L. Martín-Moreno, “In the diffraction shadow: Norton waves versus surface plasmon polaritons in the optical region,” *New Journal of Physics,* vol. 11, no. 12, p. 123020, 2009.

[37] G. Makarov, V. Novikov, and S. Rybachek, “Propagation of Electromagnetic Waves over the Earth Surface,” *Moscow: Nauka,* p. 196, 1991.

[38] Y. Rahmat-Samii, R. Mittra, and P. Parhami, "Evaluation of Sommerfeld integrals for lossy half-space problems," *Electromagnetics,* vol. 1, no. 1, pp. 1-28, 1981.

[39] P. Parhami, Y. Rahmat-Samii, and R. Mittra, “An efficient approach for evaluating Sommerfeld integrals encountered in the problem of a current element radiating over lossy ground,” *IEEE Transactions on Antennas and Propagation,* vol. 28, no. 1, pp. 100-104, 1980.

[40] K. Michalski, "On the efficient evaluation of integral arising in the sommerfeld halfspace problem," in *IEE Proceedings H (Microwaves, Antennas and Propagation)*, 1985, vol. 132, no. 5: IET, pp. 312-318.

[41] K. A. Michalski and H.-I. Lin, "On the far-zone electromagnetic field of a horizontal electric dipole over an imperfectly conducting half-space with extensions to plasmonics," *Radio Science,* vol. 53, no. 1, pp. 62-82, 2018.

[42] M. E. Nazari and W. Huang, "An analytical solution of electromagnetic radiation of a vertical dipole over a layered half-space," *IEEE Transactions on Antennas and Propagation,* vol. 68, no. 2, pp. 1181-1185, 2019.

[43] M. E. Nazari and W. Huang, "Asymptotic solution for the electromagnetic scattering of a vertical dipole over plasmonic and non-plasmonic half-spaces," *IET Microwaves, Antennas & Propagation,* 2021.

[44] R. W. King, "The circuit properties and complete fields of horizontal-wire antennas and arrays over earth or sea," *Journal of applied physics,* vol. 71, no. 3, pp. 1499-1508, 1992.

[45] W. C. Chew, *Waves and fields in inhomogeneous media*. IEEE press, 1995.

[46] N. Bleistein, "Uniform asymptotic expansions of integrals with stationary point near algebraic singularity," *Communications on Pure and Applied Mathematics,* vol. 19, no. 4, pp. 353-370, 1966.

[47] N. M. Temme, "Uniform asymptotic methods for integrals," *Indagationes Mathematicae,* vol. 24, no. 4, pp. 739-765, 2013.

[48] A. Gil, J. Segura, and N. M. Temme, "Fast and accurate computation of the Weber parabolic cylinder function W (a, x)," *IMA journal of numerical analysis,* vol. 31, no. 3, pp. 1194-1216, 2011.

[49] T. J. Cui and W. C. Chew, “Efficient evaluation of Sommerfeld integrals for TM wave scattering by buried objects,” *Journal of electromagnetic waves and applications,* vol. 12, no. 5, pp. 607-657, 1998.

[50] T. Q. Dinh, K. Goto, T. Kawano, and T. Ishihara, “Novel asymptotic solution in the transition region for transmitted wave through a plane dielectric interface,” in *2011 IEEE International Symposium on Antennas and Propagation (APSURSI)*, 2011: IEEE, pp. 2511-2514.

[51] K. A. Michalski and J. R. Mosig, “On the Complete Radiation Pattern of a Vertical Hertzian Dipole Above a Low-loss Ground,” *IEEE Journal of Microwaves.* [Submitted]

[52] C. Li, T. W. Zhang, H. Y. Wang, and X. H. Wang, “A universal expression of near-filed/far-field boundary in stratified structures,” *arXiv preprint arXiv:1504.08135,* 2015.

[53] N. Bleistein, “Uniform asymptotic expansions of integrals with many nearby stationary points and algebraic singularities,” *Journal of Mathematics and Mechanics,* vol. 17, no. 6, pp. 533-559, 1967.

[54] T. K. Sarkar and M. Salazar-Palma, “The Demise of the Hundred Year Old Mythology of the Famous Sommerfeld Sign Error Along with a Realization of the Zenneck wave and its relationship with Surface, Lateral and Leaky waves.”

[55] T. K. Sarkar *et al.*, "Electromagnetic macro modeling of propagation in mobile wireless communication: Theory and experiment," *IEEE Antennas and Propagation Magazine,* vol. 54, no. 6, pp. 17-43, 2012.

[56] T. K. Sarkar, M. N. Abdallah, M. Salazar-Palma, and W. M. Dyab, "Surface Plasmons-Polaritons, Surface Waves, and Zenneck Waves: Clarification of the terms and a description of the concepts and their evolution," *IEEE Antennas and Propagation Magazine,* vol. 59, no. 3, pp. 77-93, 2017.

[57] J. R. Wait, "The ancient and modern history of EM ground-wave propagation," *IEEE Antennas and Propagation Magazine,* vol. 40, no. 5, pp. 7-24, 1998.

[58] M. H. B. Cardoso, S. Mostarshedi, G. Baudoin, and J.-M. Laheurte, "Analytical expressions of critical distances for near-ground propagation," *IEEE Transactions on Antennas and Propagation,* vol. 66, no. 5, pp. 2482-2493, 2018.

APPENDIX A

MODIFIED SADDLE POINT METHOD

This method is suitable to evaluate the integral of the form

$$I(\Omega) = \frac{1}{\sqrt{2\pi j\Omega}} \int_C g(\xi) e^{\Omega f(\xi)} d\xi\,, \quad f(\xi) = -j\cos(\xi - \xi_s), \tag{A1}$$

for a large positive value of Ω. The function g(ξ) and f(ξ) are both analytic functions of the complex variable ξ along the integration path C in the complex ξ-plane in Figure 2.3. The general idea of the saddle point method is: the integration path C can be deformed to a new path without changing the value of the integral I(Ω) and only the short portion of the deformed path, in the vicinity of the saddle point (ξ_s), intercepting the most of the value of the integral I(Ω). The saddle point can be found by solving $f'(\xi_s) = 0$ with $f''(\xi_s) \neq 0$. The deformed path can be mapped on the real axis and the saddle point can be mapped to origin by using the transformation $f(\xi) = f(\xi_s) - s^2$, we obtain

$$I(\Omega) = \frac{e^{-j\Omega}}{\sqrt{2\pi j\Omega}} \int_C G(s) e^{-\Omega s^2} ds, \tag{A2}$$

Where

$$G(s) = g(\xi)\frac{d\xi}{ds}, \quad \frac{d\xi}{ds} = -\frac{2s}{f'(\xi)}, \tag{A3}$$

Where the pole singularity is transformed to

$$s_p = e^{-j\frac{\pi}{4}} \sqrt{1 - \sin\xi_p \sin\theta_2 - \cos\xi_p \cos\theta_2}, \tag{A4}$$

in the s-plane, the saddle point is on the origin but the integration path C and pole location are changing with θ_2, which is illustrated in Figure A1. For the case that bottom layer is plasmonic medium, the Im(s_p) can be greater than 0, when the field point is near the interface. In this case,

the SDP path surrounded the pole clockwise. Hence, the integral should consider one more term from the pole

$$-2\pi j r_p e^{-p} U\left(\mathrm{Im}\, s_p\right),\ \ p = \Omega {s_p}^2 \tag{A5}$$

Where U(.) denotes the Heaviside unit step function, p is the numerical distance and r_p is the residue of the integrand G(s)

$$r_p = \lim_{s \to s_p} (s - s_p) G(s) = \lim_{\xi \to \xi_p} (\xi - \xi_p) g(\xi). \tag{A6}$$

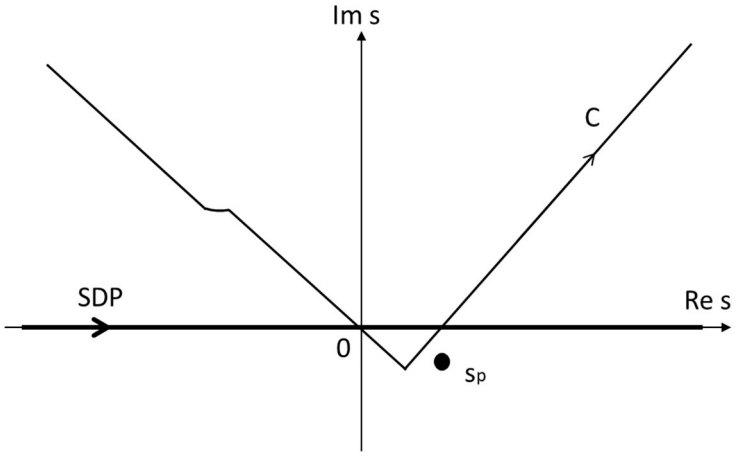

(a)

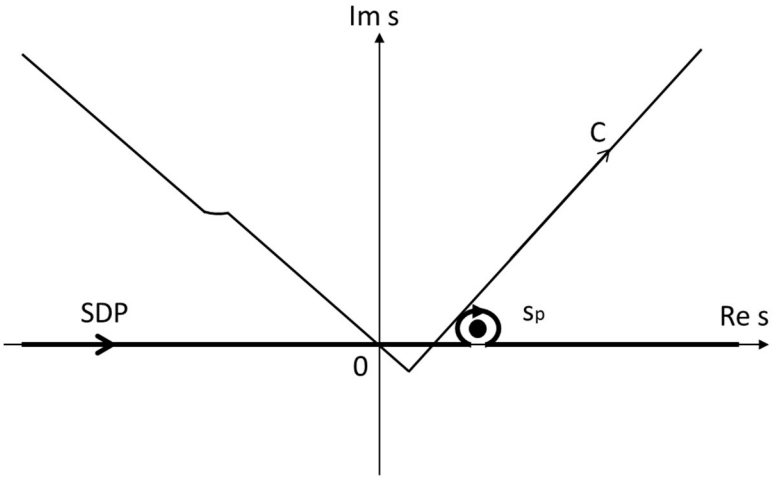

(b)

Figure A1: The integration path in s plane plots for two different θ_2 in plasmonic medium.

A.1 Subtractive Method

The idea in subtractive variant is to subtract the pole singularity from G(s) and add it back. Then G(s) can be discomposed to a regular and singularity part separately [10,11,15]. The regular part can be expanded by Maclaurin series and the singularity part can be expressed by a special function. The process is shown in the following.

In the subtractive modified saddle point method, the integrand can be approximated by

$$G(s) = \frac{r_p}{s - s_p} + [G(s) - \frac{r_p}{s - s_p}] = \frac{r_p}{s - s_p} + \sum_{n=0}^{\infty} B_n s^n, \tag{A7}$$

where

$$B_n = \frac{r_p}{{s_p}^{n+1}} + \frac{G^{(n)}(0)}{n!}. \tag{A8}$$

Substituting the approximation G(s) back into the integral, we obtain

$$I(\Omega) = \frac{e^{-\mathrm{j}\Omega}}{\sqrt{2\pi \mathrm{j}\Omega}} [r_p I_p + \sum\nolimits_{k=0}^{\infty} B_{2k} \frac{\Gamma(k + \frac{1}{2})}{\Omega^{k+\frac{1}{2}}}], \tag{A9}$$

where Γ is the gamma function and I_p can be related to the well-researched Faddeeva function [27],

$$I_p = \int_{-\infty}^{\infty} \frac{e^{-\Omega s^2}}{s - s_p} \mathrm{d}s - 2\pi \mathrm{j} e^{-p} U(\mathrm{Im}\, s_p) = -\mathrm{j}\pi\, w(-\sqrt{p}). \tag{A10}$$

and its computer subroutine is available in [27]. By using the symmetry relation w(z) + w(-z) = $2e^{-z^2}$[26], and substituting into and combining terms, we obtain

$$I(\Omega) = \frac{1}{\sqrt{2j}} \{G(0) + \sum\nolimits_{k=1}^{\infty} [\frac{r_p}{{s_p}^{2k+1}} + \frac{G^{(2k)}(0)}{(2k)!}] \frac{\Gamma(k + \frac{1}{2})}{\sqrt{\pi}\Omega^k} + \frac{r_p}{s_p} \mathcal{F}(p)\} \frac{e^{-j\Omega}}{\Omega}, \tag{A11}$$

where

$$\mathcal{F}(p) = 1 - j\sqrt{\pi \mathrm{p}}\, w(-\sqrt{p}), \tag{A12}$$

which is the attenuation function of Sommerfeld. When |p|>>1, the asymptotic expansion of the attenuation function behaves as [29]

$$\mathcal{F}(p) \sim -\frac{1}{2p}\sum_{n=0}^{\infty}\frac{(2n+1)!!}{(2p)^n} - 2j\sqrt{\pi \mathrm{p}}e^{-p}U(\mathrm{Im}\, s_p), \tag{A13}$$

where the last term attributes to the surface wave when bottom layer is plasmonic media. Even though the higher order terms can be obtained in (A11), we usually only obtain the leading order term by using the saddle point method, because it is complicated to compute the higher order derivatives of G(s) [11]. The coefficient for the first three leading order terms in (A11) is shown

$$G(0) = \sqrt{2j}g, \qquad G'(0) = 2\mathrm{jg}', \qquad G^{''}(0) = \sqrt{2j}\frac{j}{2}(g + 4g^{''}), \tag{A14}$$

where g and its derivative are evaluated at the saddle point. By keeping the first term of expansion in (A11), we obtain the first order approximation

$$I(\Omega) \sim [g + \frac{r_p}{\sqrt{2j}s_p}\mathcal{F}(p)]\frac{e^{-j\Omega}}{\Omega}, \tag{A15}$$

By keeping the first three terms of expansion in (A11), we obtain the second order approximation

$$I(\Omega) \sim g\frac{e^{-j\Omega}}{\Omega} + \frac{j}{8}(g + 4g^{''})\frac{e^{-j\Omega}}{\Omega^2} + \frac{r_p}{\sqrt{2j}s_p}\left[\mathcal{F}(p) + \frac{1}{2p}\right]\frac{e^{-j\Omega}}{\Omega}. \tag{A16}$$

Where

$$\triangle I(\Omega) \sim \frac{j}{8}(g + 4g^{''})\frac{e^{-j\Omega}}{\Omega^2} + \frac{r_p}{\sqrt{2j}s_p}\frac{1}{2p}\frac{e^{-j\Omega}}{\Omega}, \tag{A16.1}$$

is the second-order correction term.

A.2 Multiplicative Method

Similar to (A1), G(s) is multiplied and divided by ($s-s_p$) [6,8]. Then ($s-s_p$)G(s) is regular function and $1/(s-s_p)$ can be expressed by the special function.

$$G(s) = \frac{1}{s - s_p}[(s - s_p)G(s)] = \frac{1}{s - s_p}\sum_{n=0}^{\infty} A_n s^n, \tag{A17}$$

Where

$$A_n = \frac{\mathrm{n}G^{(n-1)}(0) - s_p G^{(n)}(0)}{n!}, \qquad G^{(-1)}(0) = 0. \tag{A18}$$

Using the identity

$$\frac{s^n}{s - s_p} = \sum_{k=0}^{n-1} {s_p}^k s^{n-k-1} + \frac{{s_p}^n}{s - s_p}, \tag{A19}$$

and noting that

$$\sum_{n=0}^{\infty} A_n {s_p}^n = r_p, \tag{A20}$$

we obtain

$$I(\Omega) = \frac{1}{\sqrt{2j}}\{G(0) + \sum\nolimits_{n=3}^{\infty} A_n \sum\nolimits_{k=1}^{(n-1)/2} {s_p}^{n-2k-1} \frac{\Gamma(k+\frac{1}{2})}{\sqrt{\pi}\Omega^k} + \frac{r_p}{s_p}\mathcal{F}(p)\}\frac{e^{-j\Omega}}{\Omega}. \tag{A21}$$

The double summation term has the equivalent form

$$\begin{aligned} &\sum\nolimits_{n=3}^{\infty} A_n \sum\nolimits_{k=1}^{(n-1)/2} {s_p}^{n-2k-1} \frac{\Gamma\left(k+\frac{1}{2}\right)}{\sqrt{\pi}\Omega^k} \\ &= \sum\nolimits_{k=1}^{\infty} \frac{\Gamma(k+\frac{1}{2})}{\sqrt{\pi}\Omega^k} \sum\nolimits_{n=2k+1}^{\infty} A_n {s_p}^{n-2k-1}, \end{aligned} \tag{A22}$$

And

$$\sum_{n=2k+1}^{\infty} A_n {s_p}^{n-2k-1} = (\sum_{n=0}^{\infty} - \sum_{n=0}^{2k}) A_n {s_p}^{n-2k-1} = \frac{r_p}{{s_p}^{2k+1}} + \frac{G^{(2k)}(0)}{(2k)!}. \tag{A23}$$

By keeping the first, second and third terms in [A21], we obtain the following approximations for multiplicative method:

Zeroth order approximation:

$$I(\Omega)\sim g[1-\mathcal{F}(p)]\frac{e^{-j\Omega}}{\Omega}, \tag{A24}$$

First order approximation:

$$I(\Omega)\sim[g-\sqrt{2j}s_p g'\mathcal{F}(p)]\frac{e^{-j\Omega}}{\Omega}, \tag{A25}$$

Second order approximation:

$$I(\Omega)\sim[g-j\frac{{s_p}^2}{4}(g+4g'')\mathcal{F}(p)]\frac{e^{-j\Omega}}{\Omega}. \tag{A26}$$

APPENDIX B

THE $1/R^{1.5}$ DECAY IN CELLULAR WIRELESS COMMUNICATION

The |Ez| component of electromagnet wave from a VED has -30 dB/decade along the horizontal distance in the intermediate region and -40 dB/decade in the large distance in the cellular wireless communication is reported by Sarkar [54,55] by analyzing the ground wave term of the asymptotic formula obtained by multiplicative variant of MSP method [8]. Although the -40 dB/decade decay in the far field region, which is the same as the surface wave decay derived by Norton [4], can be identified in the numerical results, the -30 dB/decade slope is buried in the intermediate region and not to be observed. Moreover, the transmitter and receiver heights and the bottom medium used in Sarkar's model make the ground wave has no significant contribution, which can also be predicted by using formula in [58]. Instead, it turns out the geometric optical terms dominates the intermediate and far field region by comparing the asymptotic results with the exact Sommerfeld integral. The subtractive type of the first-order and second-order saddle point method (Sub1 and Sub2) in (2.1) and the leading order terms of the geometric optic (1/R)

$$E_{z,1/R} = -j\frac{\eta_1 {k_1}^2}{4\pi}[\sin^2\theta_1 \frac{e^{-jk_1 r_1}}{k_1 r_1} + \Gamma_{||}\sin^2\theta_2 \frac{e^{-jk_1 r_2}}{k_1 r_2}] \tag{B1}$$

are used for computing the $|E_z|$ field.

A high contrast medium sea water with permittivity and conductivity is considered in the lower-half layer, instead of using the low contrast urban ground in Sarkar's model, to enhance the surface wave field at 1 GHz. The observation point (Rx) is 2 m away from the inter surface. Due to the height of the cellular towers is usually around 50 – 200 feet, the 15 m and 30 m are considered for the transmitter (Tx) height in the numerical results. In Figure B1, it shows the second-order method is necessary to compute the correct field values when $k_0\rho$ is small. As the $k_0\rho$ goes up, the differences between the results of the four methods are visibly indistinguishable.

Especially (B1) can be used to predict in the far field. It means the main contribution is from the geometric optic terms and the pole effect compared with the geometric optic contribution is neglectable, which is controversy with Sarkar's derivation that the ground wave term represents the -30 and -40 dB/decade in the intermediate and far field regions. In the far field, (B1) can be simplified as

$$E_{z,1/R} \sim -j\frac{\eta_1 {k_1}^2}{4\pi}\left[\frac{2}{cos\theta_2 + \frac{\sqrt{\epsilon - sin^2\theta_2}}{\epsilon}}\frac{z_s + z_f}{r_2}\frac{e^{-jk_1 r_2}}{k_1 r_2}\right], \quad \text{(B2)}$$

the $1/R^2$ decay is observed with no ground wave term involved. The oscillation in the intermediate region is from the interferences between the direct and reflected wave. Instead of decaying away from the radiating source, the wave magnitude grows initially is because both the values of $\sin\theta_1$ and $\sin\theta_2$ grow in the near region.

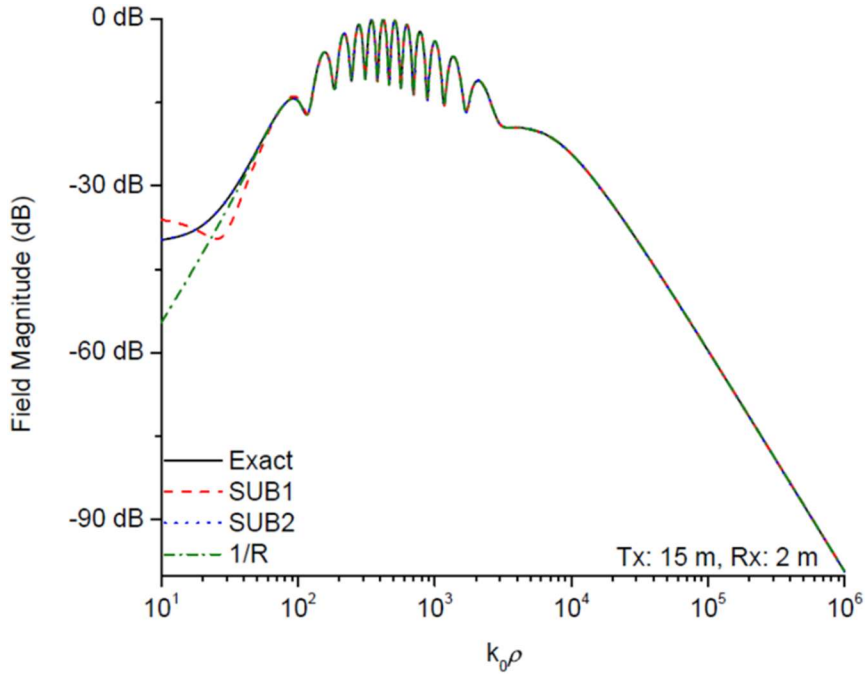

(a)

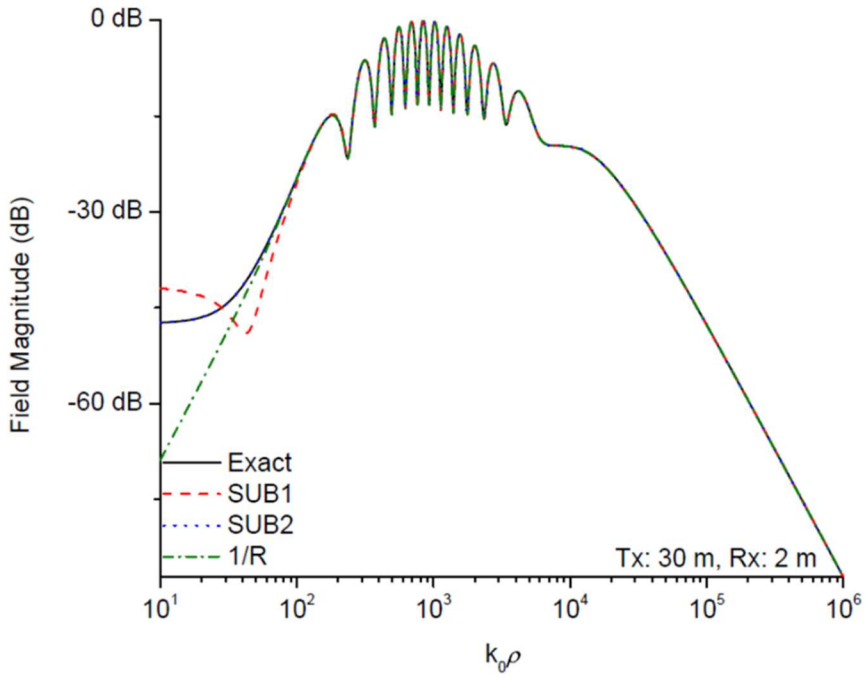

(b)

Figure B1: $|E_z|$ field along the Rx=2 m surface computed by Sub1, Sub2 and 1/R formulas and compared with the exact results in (a) Tx=15 m and (b) Tx=30 m.